IV. 研究成果の刊行物・別刷

International weekly journal of science

nature

UDP acting at $P2Y_6$ receptors is a mediator of microglial phagocytosis

Schuichi Koizumi[1,2*], Yukari Shigemoto-Mogami[1*], Kaoru Nasu-Tada[1], Yoichi Shinozaki[1,3], Keiko Ohsawa[4], Makoto Tsuda[3], Bhalchandra V. Joshi[5], Kenneth A. Jacobson[5], Shinichi Kohsaka[4] & Kazuhide Inoue[3]

[1]Division of Pharmacology, National Institute of Health Sciences, 1-18-1 Kamiyoga, Setagaya, Tokyo 158-8501, Japan. [2]Department of Pharmacology, Interdisciplinary Graduate School of Medicine and Engineering, University of Yamanashi, 1110 Shimokato, Chuo, Yamanashi 409-3893, Japan. [3]Department of Molecular and SystemPharmacology, Graduate School of Pharmaceutical Sciences, Kyushu University, 3-1-1 Maidashi, Higashi, Fukuoka 812-8582, Japan. [4]Department of Neurochemistry, National Institute of Neuroscience, 4-1-1 Ogawahigashi, Kodaira, Tokyo 187-8502, Japan. [5]Molecular Recognition Section, Laboratory of Bioorganic Chemistry, National Institute of Diabetes and Digestive and Kidney Diseases, National Institutes of Health, Bethesda, Maryland 20892-0810, USA.

**These authors contributed equally to this work.*

Reprinted from Nature, Vol. 446, No. 7139, pp. 1091–1095, 26 April 2007

LETTERS

UDP acting at $P2Y_6$ receptors is a mediator of microglial phagocytosis

Schuichi Koizumi[1,2]*, Yukari Shigemoto-Mogami[1]*, Kaoru Nasu-Tada[1], Yoichi Shinozaki[1,3], Keiko Ohsawa[4], Makoto Tsuda[3], Bhalchandra V. Joshi[5], Kenneth A. Jacobson[5], Shinichi Kohsaka[4] & Kazuhide Inoue[3]

Microglia, brain immune cells, engage in the clearance of dead cells or dangerous debris, which is crucial to the maintenance of brain functions. When a neighbouring cell is injured, microglia move rapidly towards it or extend a process to engulf the injured cell. Because cells release or leak ATP when they are stimulated[1,2] or injured[3,4], extracellular nucleotides are thought to be involved in these events. In fact, ATP triggers a dynamic change in the motility of microglia *in vitro*[5,6] and *in vivo*[3,4], a previously unrecognized mechanism underlying microglial chemotaxis[5,6]; in contrast, microglial phagocytosis has received only limited attention. Here we show that microglia express the metabotropic $P2Y_6$ receptor whose activation by endogenous agonist UDP triggers microglial phagocytosis. UDP facilitated the uptake of microspheres in a $P2Y_6$-receptor-dependent manner, which was mimicked by the leakage of endogenous UDP when hippocampal neurons were damaged by kainic acid *in vivo* and *in vitro*. In addition, systemic administration of kainic acid in rats resulted in neuronal cell death in the hippocampal CA1 and CA3 regions, where increases in messenger RNA encoding $P2Y_6$ receptors that colocalized with activated microglia were observed. Thus, the $P2Y_6$ receptor is upregulated when neurons are damaged, and could function as a sensor for phagocytosis by sensing diffusible UDP signals, which is a previously unknown pathophysiological function of P2 receptors in microglia.

Microglia express several functional P2 receptors, and their $P2X_4$, $P2X_7$ and $P2Y_{12}$ receptors have already been described in relation to their physiological and pathophysiological consequences[5–9]. To investigate the expression of mRNAs for P2 receptors that are at a higher concentration in cultured rat microglia, we conducted reverse-transcriptase-mediated polymerase chain reaction (RT–PCR) analysis with complementary DNA coding for P2Y and P2X receptors (Fig. 1a). In accordance with previous reports[5–9], microglia expressed mRNAs encoding $P2X_4$, $P2X_7$ and $P2Y_{12}$ receptors. However, we found unexpectedly that cultured rat microglia expressed a large amount of mRNA coding for $P2Y_6$ receptors, which was also confirmed by western blotting for the expression of $P2Y_6$ receptor protein (Fig. 1b). The $P2Y_6$ receptor is coupled to the activation of phospholipase C (PLC), leading to the production of inositol 1,4,5-trisphosphate ($InsP_3$) and the release of Ca^{2+} from $InsP_3$-receptor-sensitive stores[10,11]. We therefore examined changes in the intracellular Ca^{2+} concentration ($[Ca^{2+}]_i$) in microglia and found that the $P2Y_6$ receptor agonist UDP evoked increases in $[Ca^{2+}]_i$ in a concentration-dependent manner, and it also increased the fraction of the UDP-responsive cells (Supplementary Fig. 1a). The elevations in $[Ca^{2+}]_i$ induced by 100 μM UDP were significantly inhibited by the PLC inhibitor U73122, the Ca^{2+}-ATPase inhibitor in sarcoplasmic/endoplasmic reticulum thapsigargin, and the membrane-permeable $InsP_3$ receptor inhibitor xestospongin C, but were little affected by pertussis toxin (Supplementary Fig. 1b). The UDP-evoked $[Ca^{2+}]_i$ increases in microglia were significantly inhibited by reactive blue 2 (RB2), known as a potent $P2Y_6$ antagonist[11], suramin, which inhibits $P2Y_6$ receptor at higher concentrations, the diisothiocyanate derivative MRS2578, which is a selective antagonist of the $P2Y_6$ receptor[12], and an antisense oligonucleotide (AS) for $P2Y_6$ receptors, but not by a random-sequence oligonucleotide (R-oligo) (Fig. 1c). All these data show that rat microglia express functional $P2Y_6$ receptors by which UDP mobilizes Ca^{2+}.

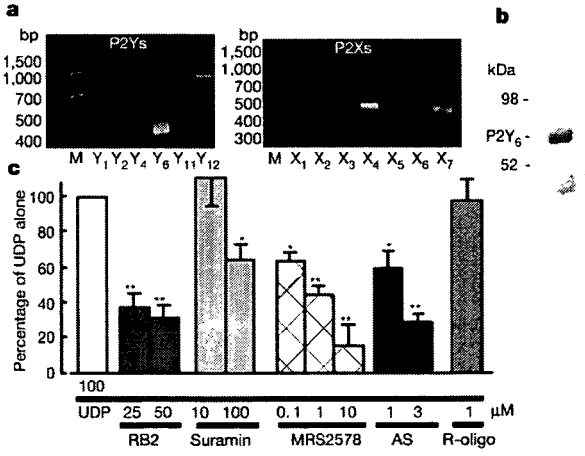

Figure 1 | Expression of $P2Y_6$ receptor and UDP-evoked increase in $[Ca^{2+}]_i$ in cultured microglia. a, RT–PCR analysis of the expression of mRNAs for $P2Y_6$, $P2Y_{12}$, $P2X_4$ and $P2X_7$ receptors in microglial cells. **b**, Expression of $P2Y_6$ receptor protein confirmed by western blotting analysis. **c**, Effects of various chemicals on the increase in $[Ca^{2+}]_i$ (measured as the change in ratio of fluorescence at 340 nm to that at 380 nm) evoked by 100 μM UDP in microglia. The maximum increase in Fura-2 fluorescence evoked by 100 μM UDP was considered as the control response, and values are expressed as a percentage of control. Data show means and s.e.m. for 24–36 cells obtained from at least three independent experiments. Significant differences from the response to UDP alone: asterisk, $P < 0.05$; two asterisks, $P < 0.01$ (Student's *t*-test).

[1]Division of Pharmacology, National Institute of Health Sciences, 1-18-1 Kamiyoga, Setagaya, Tokyo 158-8501, Japan. [2]Department of Pharmacology, Interdisciplinary Graduate School of Medicine and Engineering, University of Yamanashi, 1110 Shimokato, Chuo, Yamanashi 409-3893, Japan. [3]Department of Molecular and System Pharmacology, Graduate School of Pharmaceutical Sciences, Kyushu University, 3-1-1 Maidashi, Higashi, Fukuoka 812-8582, Japan. [4]Department of Neurochemistry, National Institute of Neuroscience, 4-1-1 Ogawahigashi, Kodaira, Tokyo 187-8502, Japan. [5]Molecular Recognition Section, Laboratory of Bioorganic Chemistry, National Institute of Diabetes and Digestive and Kidney Diseases, National Institutes of Health, Bethesda, Maryland 20892-0810, USA.
*These authors contributed equally to this work.

Morphogenesis, cell movement and phagocytosis are driven by dynamic reorganization of the actin cytoskeleton[13,14]. We showed previously that activation of $P2Y_{12/13}$ receptors, another microglial G-protein-coupled receptor, resulted in membrane ruffling and chemotaxis in microglia[5,6], and therefore we sought first to determine whether the $P2Y_6$-receptor-mediated signals affect the cell movement of microglia. Membrane ruffles are structures that are found primarily at the front edges of migrating cells[15]. To determine whether $P2Y_6$ activation stimulates microglial chemotaxis, cells were stimulated with either UDP or ATP. Neither lamellipodia-like membrane ruffles (Fig. 2a left) nor chemotaxis (Fig. 2b left) were observed when stimulated with UDP, whereas ATP produced both responses (Fig. 2a right and Fig. 2b right). However, UDP caused actin reorganization and formed aggregates of F-actin in the interior of the cells (Fig. 2a left, arrows). On stimulation with UDP (100 μM), microglia rapidly changed their morphology (Supplementary Fig. 2a); namely, to microglial processes with filopodia-like protrusions (arrows) and phagosome-like vacuoles (arrowheads). A crown-like circular structure rich in F-actins, termed the 'phagocytotic cup'[16], was also observed around the zymosan particles (Supplementary Fig. 2b, red). We speculated that UDP somehow regulates the morphogenesis of microglia, which may be involved in microglial endocytotic activities such as pinocytosis, macropinocytosis and phagocytosis. Phagocytosis is one of the most important physiological functions of microglia[17] and is the process activating the uptake of larger particles (more than 0.5 μm) by actin-based mechanisms. We investigated the UDP-evoked phagocytosis process by time-lapse videomicroscopy and flow cytometry (fluorescence-activated cell sorting; FACS)-based assay. When stimulated with 100 μM UDP, microglia rapidly phagocytosed fluorescent zymosan particles (green) (Fig. 2c, see also Supplementary Video). A quantitative phagocytosis assay by FACS shows that UDP induced the phagocytosis of latex beads in a concentration-dependent fashion (5–1,000 μM) in a 20-min incubation period (Fig. 2d). GDP (100–1,000 μM), a weak agonist of the $P2Y_6$ receptor, caused a slight uptake of microspheres (at 100 μM this was 49.7 ± 8.6% of UDP alone; $n = 4$) but ADP, also known as a weak partial agonist of the mouse $P2Y_6$ receptor, failed to stimulate the uptake (at 100 μM it was 0.3 ± 2.3% of UDP alone; $n = 4$). This is in good agreement with the previous finding that ADP does not activate rat $P2Y_6$ receptors[18]. The phagocytosis induced by 100 μM UDP was significantly inhibited by 30–100 μM RB2, a higher concentration of suramin (300 μM) and MRS2578 (0.01–3 μM), and was nearly abolished by $P2Y_6$ AS (Fig. 2e; see also Supplementary Fig. 2c, d). Recent reports indicate the existence of functional cross-talk between the nucleotides and cysteinyl leukotrienes (CysLTs, for example LTD4) in orchestrating inflammatory responses[19], indicating that some nucleotides may reveal their functions by means of a CysLT receptor (CysLTR). Microglia express a functional CysLT1R, whose activation by LTD4 resulted in an increase in $[Ca^{2+}]_i$ in microglia (Supplementary Fig. 3a). Thus, UDP acting on CysLT1R may reveal various microglial responses. However, MRS2578, a selective $P2Y_6$ receptor antagonist, did not block the LTD4-evoked Ca^{2+} responses in CysLT1R-transfected Chinese hamster ovary cells (Supplementary Fig. 3b) at a dose that inhibited the UDP-evoked increase in $[Ca^{2+}]_i$ and phagocytosis in microglia (Figs 1c and 2e). In addition, 1 μM LTD4 did not induce phagocytosis in microglia (Supplementary Fig. 3c, 4.8 ± 4.2% of that with 100 μM UDP alone; $n = 3$). All these findings suggest that the contribution of the CysLT1R to the UDP-evoked phagocytosis in microglia is negligible. Taken together, these data strongly suggest that rat microglial $P2Y_6$ receptors are coupled with phagocytic functions. The UDP-evoked phagocytosis was inhibited by 1 μM thapsigargin, the protein kinase C inhibitor staurosporin at 5 μM, and 10 μM U73122 (see Supplementary Fig. 4), indicating that activation of the $P2Y_6$ receptor seems to trigger phagocytosis through the pathway(s) mediated by PLC-linked Ca^{2+} and protein kinase C.

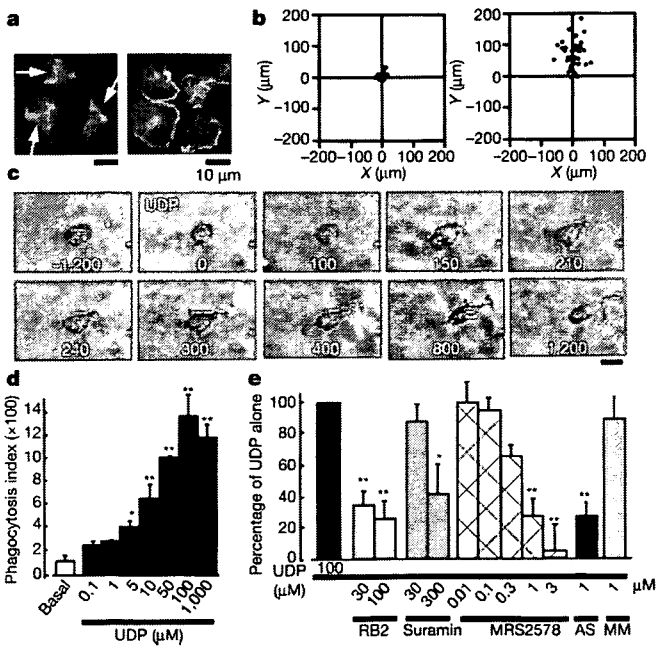

Figure 2 | Changes in cell motilities of microglia. **a**, UDP- and ATP-evoked membrane ruffles. Cultured microglia were stimulated for 5 min with 100 μM UDP (left) and 10 μM ATP (right), fixed, permeabilized, and then stained with anti-phalloidin. Scale bar, 10 μm. **b**, Typical chemotactic responses of microglia towards 100 μM UDP (left) and 100 μM ATP (right) assessed by the Dunn chemotaxis chamber (see Methods). **c**, Time-lapse images showing the effect of UDP on the microglial morphogenic changes and the uptake of fluorescent zymosan particles (green). The time after addition of UDP is shown in seconds in each picture. **d**, The UDP-evoked uptake of microspheres was assessed quantitatively as a phagocytosis index by using FACS. Data are mean and s.e.m. for three experiments (asterisk, $P < 0.05$; two asterisks, $P < 0.01$ compared with basal). **e**, Effects of the P2 receptor antagonists reactive blue 2 and suramin, the $P2Y_6$ receptor antagonist MRS2578, and $P2Y_6$ AS or MM on the UDP-evoked phagocytosis. Data are means and s.e.m. for three or four experiments (asterisk, $P < 0.05$; two asterisks, $P < 0.01$ compared with UDP alone).

Because phagocytes remove dead or damaged cells, debris and invading pathogens, recognition is the first step in phagocytosis. It is initiated by activation of the phagocytosis-promoting receptors such as Fc receptors and complement receptors[20]. In the central nervous system, microglia possess these receptors and remove amyloid-β, a key molecule in Alzheimer's disease, and attenuate Alzheimer's disease-like pathology[21]. With regard to apoptotic cells, microglia may also remove such cells by recognizing so-called 'eat-me' signals[20]. However, in the present study we used non-opsonized zymosan (Fig. 2c) and latex beads (Fig. 2d, e), which were not recognized by opsonin-dependent receptors such as Fc receptors, complement receptors or vitronectin receptors. Phagocytosis-promoting receptors also include opsonin-independent ones such as β_1-integrins, mannose receptors, scavenger receptors and phosphatidylserine receptors[13]; in fact, microglia expressed all these receptors (Supplementary Fig. 5a–e, cell lysates). Among these receptors, β_1-integrin was detected as a bead-associated protein that was slightly increased on stimulation with UDP (Supplementary Fig. 5a, bead-associated) and localized at membrane ruffle-like or phagocytic cup-like structures (see also Supplementary Fig. 2b), to which fluorescent microspheres were attached (Supplementary Fig. 5f). However, we do not know whether β_1-integrin itself binds or recognizes the microspheres. β_1-Integrin might be involved in some way in the machinery of phagocytosis or in the uptake processes of the microspheres in response to UDP, but the precise target molecule or molecules that bind or recognize microspheres to be phagocytosed remains to be identified. The microglial phagocytosis seen in the present study is a new type that is promoted by the diffusible

extracellular molecule UDP. However, we cannot deny the possibility that the UDP may simply facilitate the machinery of phagocytosis and that UDP-evoked phagocytosis observed in this study may even include macropinocytosis.

To determine the expression and function of microglial $P2Y_6$ receptors *in vivo*, the excitotoxicity of brain injury was induced by kainic acid (KA) (Fig. 3). KA is an excitatory amino acid that is often used to cause limbic motor epilepsy or excitatory neuronal cell death *in vivo* and *in vitro*. KA acts on non-NMDA glutamate receptors to facilitate excess excitability, thereby leading to necrosis and even apoptosis of neurons. The hippocampal CA1 and CA3 regions are susceptible to neuronal death in response to KA[22]. When KA was injected intraperitoneally into rats ($10\,mg\,kg^{-1}$), it produced typical limbic seizure within 60 min. At 72 h after the administration of KA, the brains were removed and were used for western blotting, immunohistochemical assays and *in situ* hybridization (ISH). Western blotting analysis showed that KA increased the expression of $P2Y_6$ receptors in comparison with the saline-injected control groups (Fig. 3A, B). Double staining of microglia and neurons by anti-Iba1 (green) and anti-neuronal nuclei (NeuN, red) antibodies, respectively, showed that KA induced severe neuronal loss in the hippocampal CA1 and CA3 regions, where intense Iba1-positive signals—indicative of microglia—were observed. KA increased the number of microglia appearing in the activated form with poorly ramified, short and thick processes (Fig. 3C, f–h). Small NeuN signals seemed to be incorporated in some microglia (see g and h in Fig. 3C), suggesting that microglia phagocytose damaged or dead neurons. These findings suggest that microglia might migrate or proliferate, probably as a result of KA-induced neuronal damage.

We further examined the cell types that produced increases in $P2Y_6$ receptor protein in response to the administration of KA, and found that $P2Y_6$ immunoreactivities (green in Fig. 3D) were associated with the microglia (OX-42, red in Fig. 3D, c) but not with astrocytes (glial fibrillary acidic protein (GFAP), red in Fig. 3D, d) or neurons (NeuN, red in Fig. 3D, e). Furthermore, we performed ISH to characterize the expression of mRNA coding for $P2Y_6$ receptors with the use of digoxigenin-labelled antisense RNA probe. Signals for $P2Y_6$ receptor mRNA were very low in the naive animals but were upregulated three days after treatment with KA (Fig. 3E, b; blue dots indicated by arrowheads). At this time, the number of microglia increased markedly, especially at the hippocampal CA3 and CA1 regions (Fig. 3C). After ISH, the sections were stained with anti-Iba1 antibody to characterize $P2Y_6$ receptor mRNA signals. In the hippocampal CA3 regions of naive rats, there were very few anti-Iba1-positive microglia that did not show $P2Y_6$ receptor mRNA. In contrast, in the hippocampal CA3 of KA-injected rats, there was an increased number of anti-Iba1-positive microglia, in which $P2Y_6$ receptor signals were colocalized with microglia (Fig. 3E, c; KA, black arrows, see also inset at higher magnification).

There is a growing literature about 'eat-me' signals that are expressed on the cell surface of apoptotic or dying cells. However, diffusible signals that trigger phagocytosis have received only limited attention. When neurons or cells are exposed to traumatic injury such as ischaemia, they swell and subsequently shrink as a result of

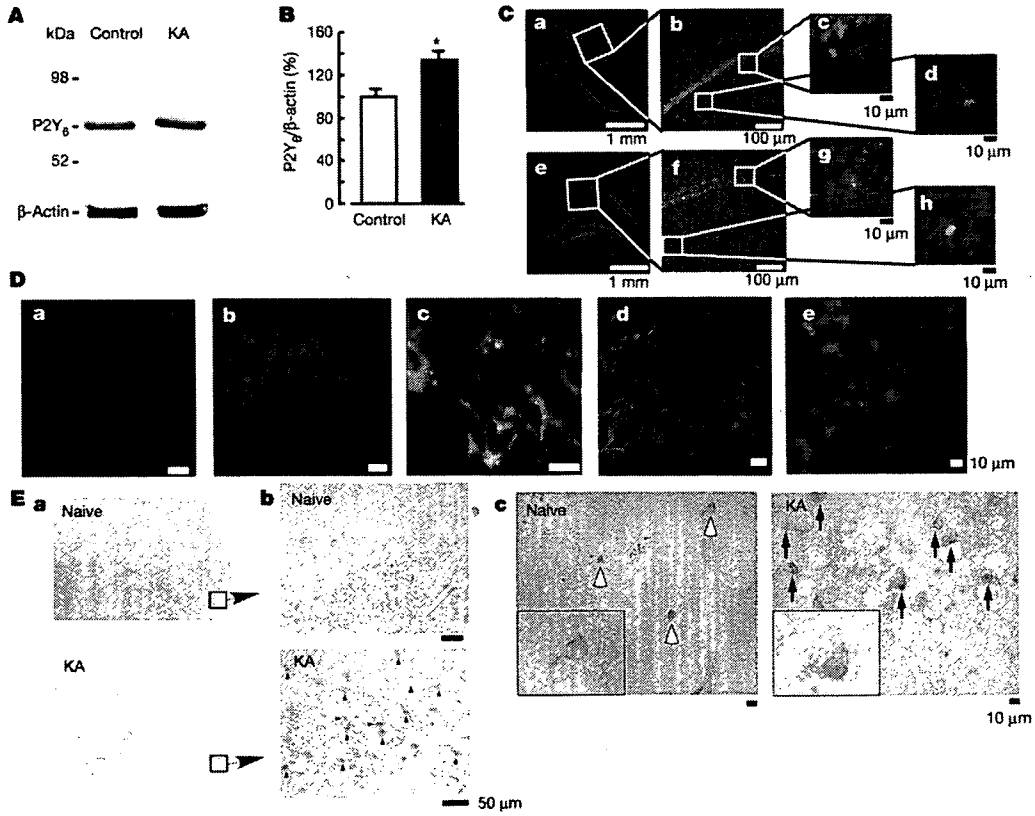

Figure 3 | Increase in $P2Y_6$ receptors in the hippocampus after kainic acid (KA)-treatment. A, Western blot analysis, showing increase in $P2Y_6$ receptor protein in rats treated intraperitoneally with $10\,mg\,kg^{-1}$ KA, 72 h after treatment. **B**, Summary of quantitative data; KA was applied at $10\,mg\,kg^{-1}$. Results are means and s.e.m. for 8 (control) and 7 (KA) experiments (asterisk, $P < 0.05$ compared with control). **C**, Immunohistochemical analysis in naive control (**a–d**) and KA-treated (**e–h**) rats; red, anti-NeuN antibody; green, anti-Iba1 antibody. Rectangles in **a** and **e** are expanded in **b** and **f**, respectively. Rectangles in **b** and **f** also correspond to **c**, **d** and **g**, **h**, respectively. **D**, Anti-$P2Y_6$ antibody signals (green) were increased by KA (**a**, control; **b**, KA), which was colocalized with microglia (red in **c**, anti-OX42) but not with astrocytes (red in **d**, anti-GFAP) or neurons (red in **e**, anti-NeuN). **E**, ISH analysis. **a**, **b**, mRNA coding for $P2Y_6$ receptor in naive rats was very low but was increased at the hippocampal CA3 region by KA (3 days later) (blue dots and arrowheads, KA). **c**, Double staining with $P2Y_6$ antisense RNA probe (blue dots) and anti-Iba-1 antibody (brown signals, white (naive) or black (KA) arrows). In KA-treated rats there was an increased number of microglia, which was associated with $P2Y_6$ receptor mRNA (blue signals, inset at higher magnification in KA).

increased permeability. This is followed by leakage of cytoplasmic molecules, leading to necrotic cell death. Thus, cytoplasmic nucleotides could be diffusible messengers that signal the crisis state to adjacent cells including microglia. In fact, the diffusible messenger ATP promotes microglial chemotaxis and/or migration[3–6]. Diffusible molecules might be insufficiently precise to cause phagocytes to recognize and eat cells. However, released or leaked nucleotides are immediately degraded by the extracellular nucleotide-degrading enzymes. In this respect, UDP might be a localized and transient marker of traumatized or necrotic cells.

Cell injury results in a leakage of ATP that affects the motility of adjacent cells, including microglia[3,4]. In addition, cells release or leak uridine nucleotides[23] and nucleotide sugars[24] in response to various stimuli or ischaemic injury[25]. We therefore next investigated whether KA increases the release of extracellular UDP from neurons to induce microglial phagocytosis. Cultured hippocampal neurons were stimulated with and without 100 μM KA for 1 h; the supernatant was then collected for nucleotide assay by high-performance liquid chromatography (HPLC) or for phagocytosis assay by FACS (Fig. 4). Because released or leaked UTP is rapidly degraded into UDP, UMP and uridine by ARL67156-sensitive ectonucleotidases, we monitored the amount of UTP rather than UDP, and collected the supernatant and the microdialysates in the presence of 20 μM ARL67156 throughout experiments. There was a close relationship between the HPLC peak corresponding to UTP and the concentration of the standard UTP ($R^2 = 0.9947$). The amount of UTP in the KA-treated supernatant was significantly larger than that in the KA-untreated control supernatant (Fig. 4b; control, 2.3 ± 1.1 μM; KA treated, 10.5 ± 3.9 μM, $P < 0.05$). We also tested whether the KA-treated supernatant obtained from cultured hippocampal neurons facilitated microglial phagocytosis. Hippocampal neurons were treated with and without 100 μM KA for 1 h; each supernatant was collected and added to microglia; this was followed by a phagocytosis assay. As shown in Fig. 4c, when microglia were incubated with the KA-treated supernatant for 20 min, there was a significant increase in phagocytosis, which was blocked by the $P2Y_6$ receptor antagonist MRS2578 (1 μM). KA alone did not stimulate phagocytosis.

Finally, we tested whether KA induces the release of UDP and $P2Y_6$-receptor-mediated phagocytosis *in vivo*. An increase in extracellular UTP concentration ($[UTP]_o$) was observed soon after injection of KA (from 1 to 4 h after injection), which reached 2–3-fold higher than the KA-untreated control (data not shown). At 1 day after KA injection, $[UTP]_o$ was about 1.5–2.0-fold higher than the KA-untreated control (Fig. 4e). Then, at day 3, $[UTP]_o$ reached almost 10-fold higher levels (9.4 ± 1.2-fold; Fig. 4e and inset), which decreased slightly at day 5. A higher (5–10-fold) $[UTP]_o$ was observed 2–3 days after the injection of KA, which lasted at least another couple of days. It should be noted that loss of neurons (removal of neurons) also became obvious 2–3 days after the KA injection. We further injected fluorescent microspheres into the hippocampal CA3 regions of KA-treated rats, and then counted the numbers of the microspheres phagocytosed or attached by microglia. The $P2Y_6$ receptor antagonist MRS2578 was injected into the hippocampal CA3 region, and $P2Y_6$ AS or MM (mismatch oligonucleotide) was injected into the third ventricle. The number of microspheres taken or attached by microglia was markedly increased by KA treatment, which is significantly inhibited by MRS2578 or $P2Y_6$ AS but not by MM (Fig. 4g; see also Supplementary Fig. 6). These findings all suggest that UDP/$P2Y_6$-receptor-mediated signals are important for microglial phagocytosis even *in vivo*.

A recent review described that dying cells use both 'find-me' and 'eat-me' signals for phagocyte attraction and recognition[26]. Nucleotides could be both 'find-me' and 'eat-me' signals. The intracellular ATP concentration is estimated to be high (more than 5 mM) and the UTP concentration is reported to be one-third that of ATP[23]. Cells release ATP, and here we showed that KA caused an increase in extracellular UTP or UDP. Microglia might therefore be attracted by ATP or ADP[5,6] and subsequently recognize UDP, leading to the removal of the dying cells or their debris. It is interesting that ATP/ADP is not able to efficiently activate $P2Y_6$ receptors; neither can UDP act on $P2Y_{12/13}$ receptors. Thus, even if these nucleotides were leaked or released simultaneously, adenine and uridine nucleotides would regulate microglial motilities, namely chemotaxis and phagocytosis, in a mutually exclusive but coordinated fashion.

So far we have not shown quantitative data indicating that individual microglia upregulate the expression of $P2Y_6$ receptors. A significant, but not drastic, increase in $P2Y_6$ receptor protein in the hippocampus was observed after injection of KA (Fig. 3A, B). ISH data show that expression of mRNA coding for $P2Y_6$ receptors in microglia was very low in naive animals but became obvious in an increased number of microglia after KA injection (Fig. 3E), suggesting that the increase in $P2Y_6$ receptor protein is not due simply to an increased number of microglia but is upregulated in individual

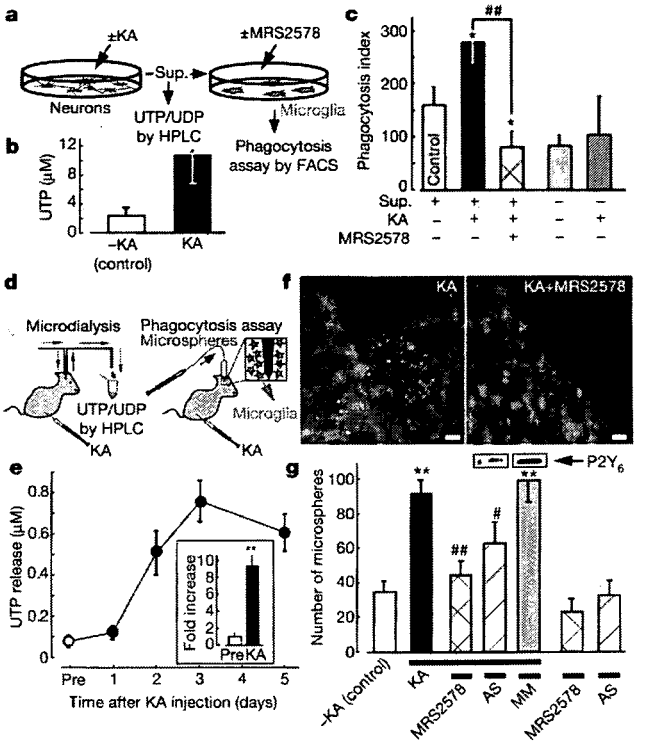

Figure 4 | KA-evoked increases in extracellular uridine nucleotides and $P2Y_6$-receptor-mediated microglial phagocytosis *in vitro* and *in vivo*. **a**, Schematic diagram of the experiments *in vitro*. Sup., supernatant. **b**, Summary of the UTP concentration in the KA-treated and control supernatants. Data show means and s.e.m. for at least five independent experiments (asterisk, $P < 0.05$ compared with control). **c**, Effects of the KA-treated and control supernatant on microglial uptake of fluorescent latex beads. Data show means and s.e.m. for at least four independent experiments (asterisk, $P < 0.05$ compared with control; hash sign, $P < 0.05$ compared with KA-treated supernatant). **d**, Schematic diagram of the experiments *in vivo*. KA was applied intraperitoneally at 10 mg kg^{-1}. **e**, Time course of changes in $[UTP]_o$ in baseline dialysates (before treatment with KA (Pre), and 1, 2, 3 and 5 days afterwards). Inset, fold increase at day 3 (compared with before treatment). **f**, Typical pictures of fluorescent microspheres (green) attached or taken up by microglia (red, anti-Iba1) in the KA-treated (left) and KA + MRS2578-treated (right) hippocampal CA3 regions. Scale bar, 20 μm. **g**, Quantitative analysis of phagocytosis *in vivo* (details are provided in Supplementary Methods). Changes in $P2Y_6$ receptor protein by $P2Y_6$ AS or MM are shown at the top of corresponding columns. Values are means and s.e.m. (asterisk, $P < 0.01$ compared with control (−KA); hash sign, $P < 0.05$; two hash signs, $P < 0.01$ compared with KA-treated group). Statistical analyses were performed by ANOVA with Scheffe's multiple comparison. At least three sections containing the injection sites were analysed per animal, and at least three animals were used in each group for analysis.

microglia. We also emphasize that even if the extent of $P2Y_6$ receptor upregulation is not drastic, an increase in extracellular UDP, a ligand for $P2Y_6$ receptor, is markedly increased after treatment with KA (detected as UTP, almost 10-fold; Fig. 4e) and therefore that the UDP/$P2Y_6$ receptor system would be sufficiently activated to cause microglial phagocytosis after treatment with KA. In comparison with the extensive knowledge of the molecular events involved in the regulation of apoptosis or necrosis, relatively little is known about the processes responsible for the clearance of dead cells and the degradation of waste materials. Considering the present findings that injured neurons leak diffusible UTP/UDP and cause the upregulation of $P2Y_6$ receptors in microglia, the UDP/$P2Y_6$ receptor system might function as a critical device covering the phagocytosis of both apoptotic and necrotic cells if they release or leak UDP by sensing diffusible UDP signals.

Thus we have shown that microglia express $P2Y_6$ receptors that function as a sensor of phagocytosis. The $P2Y_6$ receptor agonist UDP is released (as UTP) when neurons are damaged by KA. Thus, the activation of $P2Y_6$ receptors by UDP would be a key event in initiating the clearance of dying cells or debris in the central nervous system.

METHODS

Detailed methods are provided in Supplementary Information.

Microglia culture. The protocol was reviewed and approved by the Committee for Institutional Laboratory Animal Care of the National Institute of Health Sciences. Rat primary cultured microglia were prepared in accordance with the method described previously[27].

Phagocytosis assay *in vitro* and *in vivo*. *In vitro* microglial phagocytosis was assessed by either FACScan analysis or imaging analysis with fluorescently labelled microspheres. For the *in vivo* phagocytosis assay, fluorescently labelled microspheres were injected into the hippocampal CA3 region after injection of KA, and then the number of fluorescent microspheres associated with microglia was analysed by confocal microscopy (LSM 5 Pascal; Carl Zeiss).

Microdialysis. A microdialysis probe (A-I type probe; Eicom) was inserted into the hippocampal CA3 region by means of a guide cannula, and was perfused continuously at a flow rate of 3.0 $\mu l\ min^{-1}$ (collected for 60 min) supplemented with the ectonuclease inhibitor ARL67156 (20 μM) (Sigma).

Quantification of UTP by HPLC. The concentration of nucleotides in the supernatant of the hippocampal cultures was analysed with an HPLC system (Jasco) combined with a C_{18} column (4.6 × 250 mm, Shodex) as described[28], with minor modifications.

Data analysis and statistics. All results are expressed as means ± s.e.m. A statistical analysis was performed with Student's *t*-test or analysis of variance, followed by Scheffe's multiple comparison test. Differences were considered to be significant at $P < 0.05$.

Received 23 December 2006; accepted 23 February 2007.
Published online 4 April 2007.

1. Guthrie, P. B. *et al.* ATP released from astrocytes mediates glial calcium waves. *J. Neurosci.* **19**, 520–528 (1999).
2. Koizumi, S., Fujishita, K., Tsuda, M., Shigemoto-Mogami, Y. & Inoue, K. Dynamic inhibition of excitatory synaptic transmission by astrocyte-derived ATP in hippocampal cultures. *Proc. Natl Acad. Sci. USA* **100**, 11023–11028 (2003).
3. Nimmerjahn, A., Kirchhoff, F. & Helmchen, F. Resting microglial cells are highly dynamic surveillants of brain parenchyma *in vivo*. *Science* **308**, 1314–1318 (2005).
4. Davalos, D. *et al.* ATP mediates rapid microglial response to local brain injury *in vivo*. *Nature Neurosci.* **8**, 752–758 (2005).
5. Honda, S. *et al.* Extracellular ATP or ADP induce chemotaxis of cultured microglia through $G_{i/o}$-coupled P2Y receptors. *J. Neurosci.* **21**, 1975–1982 (2001).
6. Nasu-Tada, K., Koizumi, S. & Inoue, K. Involvement of β1 integrin in microglial chemotaxis and proliferation on fibronectin: different regulations by ADP through PKA. *Glia* **52**, 98–107 (2005).
7. Ferrari, D. *et al.* P2Z purinoreceptor ligation induces activation of caspases with distinct roles in apoptotic and necrotic alterations of cell death. *FEBS Lett.* **447**, 71–75 (1999).
8. Suzuki, T. *et al.* Production and release of neuroprotective tumor necrosis factor by P2X7 receptor-activated microglia. *J. Neurosci.* **24**, 1–7 (2004).
9. Tsuda, M. *et al.* P2X4 receptors induced in spinal microglia gate tactile allodynia after nerve injury. *Nature* **424**, 778–783 (2003).
10. Chang, K., Hanaoka, K., Kumada, M. & Takuwa, Y. Molecular cloning and functional analysis of a novel P2 nucleotide receptor. *J. Biol. Chem.* **270**, 26152–26158 (1995).
11. Communi, D., Parmentier, M. & Boeynaems, J. M. Cloning, functional expression and tissue distribution of the human P2Y6 receptor. *Biochem. Biophys. Res. Commun.* **222**, 303–308 (1996).
12. Mamedova, L. K., Joshi, B. V., Gao, Z. G., von Kugelgen, I. & Jacobson, K. A. Diisothiocyanate derivatives as potent, insurmountable antagonists of P2Y6 nucleotide receptors. *Biochem. Pharmacol.* **67**, 1763–1770 (2004).
13. Greenberg, S. Signal transduction of phagocytosis. *Trends Cell Biol.* **5**, 93–99 (1995).
14. Mitchison, T. J. & Cramer, L. P. Actin-based cell motility and cell locomotion. *Cell* **84**, 371–379 (1996).
15. Lauffenburger, D. A. & Horwitz, A. F. Cell migration: a physically integrated molecular process. *Cell* **84**, 359–369 (1996).
16. Ohsawa, K., Imai, Y., Kanazawa, H., Sasaki, Y. & Kohsaka, S. Involvement of Iba1 in membrane ruffling and phagocytosis of macrophages/microglia. *J. Cell Sci.* **113**, 3073–3084 (2000).
17. Kreutzberg, G. W. Microglia: a sensor for pathological events in the CNS. *Trends Neurosci.* **19**, 312–318 (1996).
18. Nicholas, R. A. *et al.* Pharmacological and second messenger signalling selectivities of cloned P2Y receptors. *J. Auton. Pharmacol.* **16**, 319–323 (1996).
19. Mellor, E. A., Maekawa, A., Austen, K. F. & Boyce, J. A. Cysteinyl leukotriene receptor 1 is also a pyrimidinergic receptor and is expressed by human mast cells. *Proc. Natl Acad. Sci. USA* **98**, 7964–7969 (2001).
20. Lauber, K. *et al.* Apoptotic cells induce migration of phagocytes via caspase-3-mediated release of a lipid attraction signal. *Cell* **113**, 717–730 (2003).
21. Bard, F. *et al.* Peripherally administered antibodies against amyloid β-peptide enter the central nervous system and reduce pathology in a mouse model of Alzheimer disease. *Nature Med.* **6**, 916–919 (2000).
22. Sperk, G. *et al.* Kainic acid induced seizures: neurochemical and histopathological changes. *Neuroscience* **10**, 1301–1315 (1983).
23. Lazarowski, E. R., Homolya, L., Boucher, R. C. & Harden, T. K. Direct demonstration of mechanically induced release of cellular UTP and its implication for uridine nucleotide receptor activation. *J. Biol. Chem.* **272**, 24348–24354 (1997).
24. Lazarowski, E. R., Shea, D. A., Boucher, R. C. & Harden, T. K. Release of cellular UDP-glucose as a potential extracellular signaling molecule. *Mol. Pharmacol.* **63**, 1190–1197 (2003).
25. Erlinge, D. *et al.* Uridine triphosphate (UTP) is released during cardiac ischemia. *Int. J. Cardiol.* **100**, 427–433 (2005).
26. Ravichandran, K. S. 'Recruitment signals' from apoptotic cells: invitation to a quiet meal. *Cell* **113**, 817–820 (2003).
27. Nakajima, K. *et al.* Identification of elastase as a secretory protease from cultured rat microglia. *J. Neurochem.* **58**, 1401–1408 (1992).
28. Lazarowski, E. R., Boucher, R. C. & Harden, T. K. Constitutive release of ATP and evidence for major contribution of ecto-nucleotide pyrophosphatase and nucleoside diphosphokinase to extracellular nucleotide concentrations. *J. Biol. Chem.* **275**, 31061–31068 (2000).

Supplementary Information is linked to the online version of the paper at www.nature.com/nature.

Acknowledgements We thank T. Shimizu and Dr. S. Ishii for providing CysLT1 receptor-expressed Chinese hamster ovary cells; K. Sakemi for technical assistance; Y. Sasaki for helpful suggestions; K. Suzuki and R. Adachi for allowing us to use the Pascal confocal microscope system; and T. Nishimaki-Mogami, Y. Ohno and T. Nagao for continuous encouragement. This study was supported in part by a grant from The National Institute of Biomedical Innovation, a grant from Uehara Memorial Foundation, a Grant-in-Aid for Scientific Research on Priority Areas, for Creative Scientific Research, Scientific Research (A and B), and for Young Scientists (A) from the Ministry of Education, Science, Sports and Culture of Japan.

Author Contributions S.K. designed most experiments, performed Ca^{2+} imaging and *in vivo* experiments and wrote the paper. Y.S.M. conducted major parts of the experiments. K.N.T. and Y.S. carried out the FACS assay and the HPLC analysis, respectively. K.O. and S.K. performed the chemotaxis analysis. B.V.J. and K.A.J. made the $P2Y_6$ receptor antagonist MRS2578. M.T. analysed the data. K.I. analysed the data and coordinated the project. K.I. also designed the project. All authors discussed the results and commented on the manuscript.

Author Information Reprints and permissions information is available at www.nature.com/reprints. The authors declare no competing financial interests. Correspondence and requests for materials should be addressed to K.I. (inoue@phar.kyushu-u.ac.jp).

Cell

SCRAPPER-Dependent Ubiquitination of Active Zone Protein RIM1 Regulates Synaptic Vesicle Release

Ikuko Yao,[1] Hiroshi Takagi,[1] Hiroshi Ageta,[1] Tomoaki Kahyo,[1] Showbu Sato,[1] Ken Hatanaka,[1] Yoshiyuki Fukuda,[2] Tomoki Chiba,[3,7] Nobuhiro Morone,[4] Shigeki Yuasa,[4] Kaoru Inokuchi,[1] Toshihisa Ohtsuka,[5] Grant R. MacGregor,[6] Keiji Tanaka,[3] and Mitsutoshi Setou[1,2,*]

[1]Mitsubishi Kagaku Institute of Life Sciences (MITILS), 11 Minamiooya, Machida, Tokyo 194-8511, Japan

[2]National Institute for Physiological Sciences, 5-1 Higashiyama, Myodaiji-cho, Okazaki, Aichi 444-8787, Japan

[3]Laboratory of Frontier Science, The Tokyo Metropolitan Institute of Medical Science, 3-18-22 Honkomagome, Bunkyo-ku, Tokyo 113-8613, Japan

[4]Department of Ultrastructural Research, National Institute of Neuroscience, National Center of Neurology and Psychiatry, 4-1-1 Ogawahigashi-cho, Kodaira, Tokyo 187-8502, Japan

[5]Department of Clinical and Molecular Pathology, Faculty of Medicine/Graduate School of Medicine, University of Toyama, Sugitani 2630, Toyama 930-0194, Japan

[6]Department of Developmental and Cell Biology, and Center for Molecular and Mitochondrial Medicine and Genetics, University of California, Irvine, CA 92697-3940, USA

[7]Present address: University of Tsukuba, Graduate School of Life and Environmental Sciences, 1-1-1 Tennodai, Tsukuba, Ibaraki 305-8577, Japan.

*Correspondence: setou@nips.ac.jp

DOI 10.1016/j.cell.2007.06.052

SUMMARY

Little is known about how synaptic activity is modulated in the central nervous system. We have identified SCRAPPER, a synapse-localized E3 ubiquitin ligase, which regulates neural transmission. SCRAPPER directly binds and ubiquitinates RIM1, a modulator of presynaptic plasticity. In neurons from *Scrapper*-knockout (SCR-KO) mice, RIM1 had a longer half-life with significant reduction in ubiquitination, indicating that SCRAPPER is the predominant ubiquitin ligase that mediates RIM1 degradation. As anticipated in a RIM1 degradation defect mutant, SCR-KO mice displayed altered electrophysiological synaptic activity, i.e., increased frequency of miniature excitatory postsynaptic currents. This phenotype of SCR-KO mice was phenocopied by RIM1 overexpression and could be rescued by re-expression of SCRAPPER or knockdown of RIM1. The acute effects of proteasome inhibitors, such as upregulation of RIM1 and the release probability, were blocked by the impairment of SCRAPPER. Thus, SCRAPPER has an essential function in regulating proteasome-mediated degradation of RIM1 required for synaptic tuning.

INTRODUCTION

During neuronal communication, synaptic vesicles dock and fuse with the plasma membrane of the presynaptic (transmitting) neuron at sites called "active zones." Subsequently, neurotransmitters released into the extracellular synaptic space can bind to cell surface receptors located at sites on the postsynaptic (receiving) cell called "postsynaptic densities." Both of these specialized intracellular sites contain complexes of scaffolding proteins, neurotransmitter-releasing machinery, receptors, ion channels, and signaling molecules that facilitate synaptic transmission and subsequent signal transduction (Hata and Takai, 1999; Sudhof, 2004; Yao et al., 1999). Modulation of the activity of such protein complexes is important for control of synaptic plasticity. It is not yet fully understood how the activity of these synaptic proteins is regulated, but this sophisticated process includes control at the level of transcription (Bito et al., 1996), translation (Kosik, 2006), and translocation (Ikegami et al., 2007; Matsumoto et al., 2007; Setou et al., 2000, 2002).

Recently, protein degradation has attracted attention as a mechanism to control the level of synaptic proteins. Protein degradation mediated by the ubiquitin-proteasome system (UPS) (Coux et al., 1996; Hershko and Ciechanover, 1998; Varshavsky, 2005) functions in a variety of cellular processes (Pickart, 2001; Varshavsky, 2005). Target proteins are tagged with polyubiquitin via UPS enzymes and then degraded in the proteasome. By controlling the stability, activity, and localization of

synaptic proteins, UPS provides an additional mechanism for control of synaptic function. For example, UPS machinery can modulate the level of synaptic proteins such as Vesl-1S/Homer-1a (Ageta et al., 2001), serum-inducible kinase (SNK) (Pak and Sheng, 2003), anaplastic lymphoma kinase (ALK) (Liao et al., 2004), synaptophysin (Wheeler et al., 2002), and syntaxin1 (Chin et al., 2002). Furthermore, it has been suggested that activity-dependent regulation of synaptic function in vivo can be regulated by UPS at both pre- and postsynapses (Ehlers, 2003; Yi and Ehlers, 2005). Indeed, optical analysis of synaptic vesicles indicates that inhibition of proteasome activity triggers a presynaptic modulation in cultured hippocampal neurons (Willeumier et al., 2006). However, the molecular mechanisms whereby UPS regulates synaptic transmission in vivo are unknown.

We have identified SCRAPPER, an ubiquitin ligase found in mammalian CNS synapses and have analyzed its function in synaptic transmission. SCRAPPER directly binds to and ubiquitinates the active zone protein Rab3-interacting molecule 1 (RIM1) in vitro and in vivo. Analysis of mice mutant for SCRAPPER demonstrates that SCRAPPER-dependent UPS contributes to the regulation of synaptic vesicle release probability via RIM1.

RESULTS

SCRAPPER Is a Neural E3 Ubiquitin Ligase Localized on Presynaptic Membrane

Protein ubiquitination involves three classes of enzymes: ubiquitin-activating enzyme (E1), ubiquitin-conjugating enzymes (E2), and ubiquitin-protein ligases (E3). Specificity in ubiquitination is often conferred by E3 enzymes due to their high-substrate specificity. We hypothesized that an E3 capable of regulating synaptic function would be membrane bound and would be expressed in neurons. To test this hypothesis we screened the human genome for genes whose coding sequence contained an F box domain (characteristic of E3 ligases), a membrane-targeting sequence, and whose promoter region contained both a neuron-restrictive silencing element and a cAMP-response element (CRE) within 3 kb upstream of exon 1. Only one gene was found with all of these properties. We cloned a full-length cDNA for the mouse ortholog and named the encoded protein "SCRAPPER." SCRAPPER is a 438 amino acid protein that contains an F box, leucine-rich repeats (LRR), and a CAAX domain. The CAAX domain is a carboxyl-terminal membrane-sorting signal induced by prenylation (Zhang and Casey, 1996).

We verified that SCRAPPER has these properties in vivo. Cyclic-AMP responsive expression of *Scrapper* mRNA was observed in primary culture of hippocampal neurons 1 hr following induction by forskolin (a cAMP signaling activator) (Figure S1). Western analysis of levels of SCRAPPER in the mouse brain revealed a gradual increase with age, from midgestation to adult (Figure S2A). In adult mice, highest levels of SCRAPPER were observed in the brain (Figure 1A), where it appeared evenly distributed (Figure S2B). Analysis using in situ hybridization (Figure 1B) and immunohistochemistry (Figure 1C) revealed that *Scrapper* mRNA and protein were enriched in the CA1, CA3, and dentate gyrus regions of the hippocampus, as well as in the cerebellum and olfactory bulb. Subcellularly, SCRAPPER was enriched in synaptic membrane fractions from the mouse brain (Figure 1D). Immunofluorescence analysis revealed a punctate distribution of SCRAPPER (Figure 1F) that predominantly colocalized with synaptophysin, a known synaptic vesicle protein and presynapse marker. GFP-tagged full-length SCRAPPER (GFP-SCR) was distributed in a punctate manner similar to endogenous SCRAPPER (Figures 1E and 1F). In contrast, GFP-SCR-C435A, which carries a mutation in the CAAX motif, had more diffuse distribution than those observed for wild-type GFP-SCR and -SCR-CAAX. This indicates that the carboxyl-terminal prenylation signal is important for the distinct localization of SCRAPPER. GFP-SCR-LRR, which we expected to have a dominant-negative effect due to presence of the LRR target protein-binding domain, but without the F box or CAAX domains, also displayed a diffuse subcellular distribution (Figure 1F).

SCRAPPER Acts as an E3 Ubiquitin Ligase for RIM1 In Vitro

F box-containing proteins are a component of the multisubunit RING-finger type SCF complex (Cardozo and Pagano, 2004), which acts as an E3 enzyme. Similarly, SCRAPPER formed an SCF complex with Skp1 and Cullin1 in mouse brain lysates (Figure 2A). Consistent with a function as a ubiquitin ligase, ubiquitinated proteins coimmunoprecipitated (co-IPed) with FLAG-tagged SCRAPPER (FLAG-SCR) from lysates of MG132-treated (a proteasome inhibitor) cells (Figure 2B). These ubiquitinated proteins may include target proteins and/or autoubiquitinated SCRAPPER. Due to the colocalization of SCRAPPER with synaptophysin (Figure 1F), we screened the SCRAPPER IPs for known presynaptic proteins (Figure 2C). RIM1, a Ca^{2+}-dependent synaptic vesicle-priming factor in the active zone that is required for synaptic plasticity (Wang et al., 1997), co-IPd with SCRAPPER (Figure 2C). SCRAPPER partially colocalized with RIM1 in cultured neurons (Figure 2D). Purified recombinant SCRAPPER and C2B domain of RIM1 directly interacted in an in vitro pull-down assay (Figures 2E and S3). Furthermore, in IPs of native SCRAPPER from the mouse brain, RIM1 was shifted to a higher molecular weight after the addition of a ubiquitination priming mixture (E1, E2, ubiquitin, and a NEDD8 system [Kawakami et al., 2001]) (Figure 2F). Thus, the SCRAPPER complex was sufficient to mediate ubiquitination of RIM1 in vitro.

SCR-KO Mice Have Deficiency in RIM1 Ubiquitination, Prolonged Half-Life of RIM1, and Increased Steady-State Levels of RIM1

To investigate the physiological function of SCRAPPER, we generated *Scrapper*-knockout (SCR-KO)- and *Scrapper*-transgenic (SCR-TG) mice in which the expression

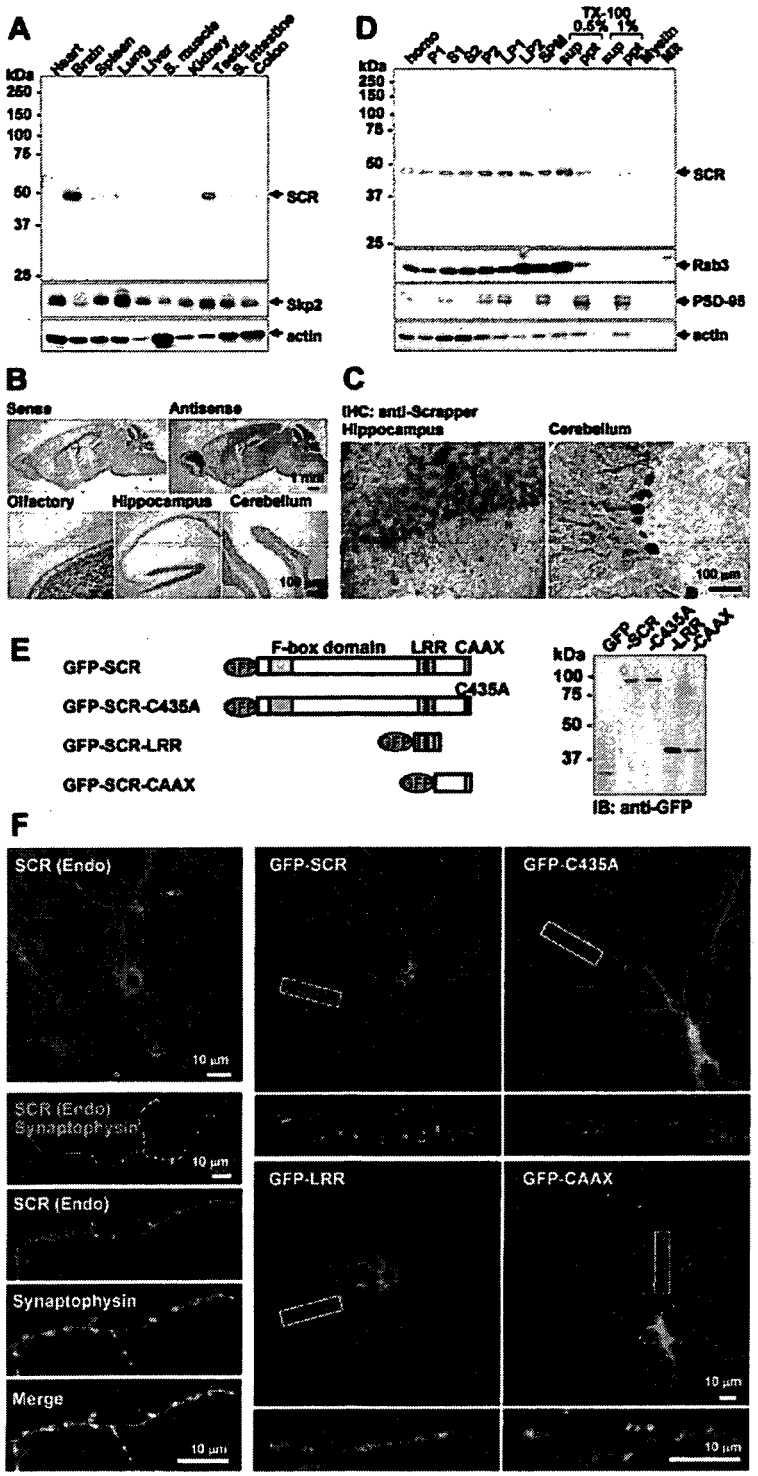

Figure 1. SCRAPPER Is a Neuronal E3 Ligase

(A) Tissue distribution of SCRAPPER protein.

(B) In situ hybridization analysis of *Scrapper* mRNA.

(C) Immunohistochemical analyses of SCRAPPER distribution in mouse cerebellum and hippocampus.

(D) Subcellular distribution of SCRAPPER in the brain. SCRAPPER was present in membrane fractions, especially synaptosomal membrane (SPM) fraction and the 0.5% (w/v) Triton X-100-soluble fraction of the SPM. Homo, the homogenate fraction. In (A) and (D), 10 μg protein was applied to each lane. Skp2, actin, Rab3, and PSD-95 are loading controls.

(E) Cartoon of GFP-tagged SCRAPPER constructs. Expression was verified using anti-GFP antibody.

(F) Shown in the left column is immunofluorescence of endogenous SCRAPPER (SCR, green) and synaptophysin (red) in cultured hippocampal neurons. Shown in the right-hand side in two columns is localization of GFP-SCR shown in (E); areas white rectangular boxes are shown at higher magnification under the respective panel.

of SCRAPPER was either abolished in all tissues or enhanced within the hippocampus, respectively (Figures 3A and 3B). No overt physiological difference was observed between SCR-TG and non-TG mice (Figures 3C and 3D, right). In contrast, the genotypes of offspring from intercross of SCR-KO heterozygous parents did not conform to a Mendelian ratio (29% wild-type [WT], 52% heterozygotes, and 19% homozygotes at birth, $p < 0.01$, χ^2 goodness-of-fit t test; Figure 3C). SCR-KO progeny also died stochastically after birth and had reduced

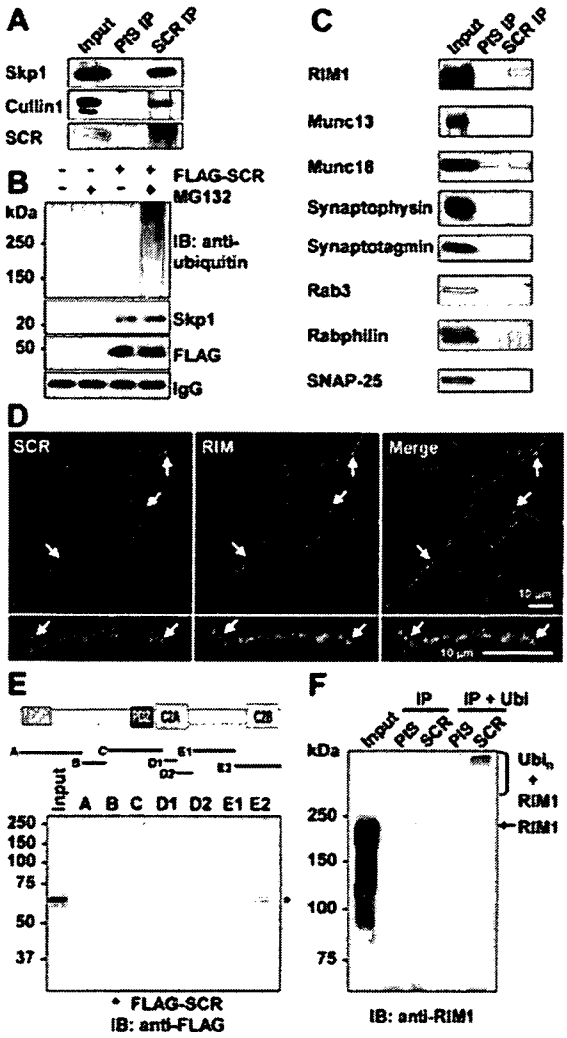

Figure 2. SCRAPPER Acts as an E3 Ligase for RIM1 In Vitro

(A) SCRAPPER forms an SCF complex in the mouse brain. Input, original tissue extract; PIS IP and SCR IP, immunoprecipitates generated using the preimmune serum (PIS IP) or with the anti-SCRAPPER antibody (SCR IP); IB, immunoblotted with indicated antibody.

(B) Extract of HEK293T cells transfected FLAG-SCR with HA-tagged ubiquitin and treated ±MG132 was immunoprecipitated with anti-FLAG antibody, and blotted with antibodies to Ubiquitin, Skp1 or FLAG.

(C) Immunoprecipitates generated with the anti-SCRAPPER antibody from the mouse brain were blotted with the indicated antibodies. Endogenous RIM1 was coimmunoprecipitated with SCRAPPER.

(D) Immunostaining pattern of endogenous SCRAPPER (SCR; green) and RIM1 (red) in cultured hippocampal neurons. Arrows indicate examples of overlapping signals.

(E) SCRAPPER interacted with the C2B domain of RIM1.

(F) Ubiquitination of RIM1 in anti-SCRAPPER immunoprecipitates. Samples were blotted with anti-RIM1 antibody. IP + Ubi, samples to which ubiquitination-system mixture (containing ubiquitin, E1, E2, and a NEDD8 system) was added to immunoprecipitates containing SCRAPPER.

lifespan (Figure 3C) and smaller body size (Figures 3D [left], S4A, and S4B) compared to WT littermates. Necropsy of homozygous SCR-KO mice was unremarkable except for a smaller pancreas (Figure S4D).

We used SCR-KO mice to investigate SCRAPPER-dependent RIM1 ubiquitination in vivo. In hippocampal acute slices prepared from WT mice, the steady-state level of RIM1 was increased by treatment (50 μM, 1 hr) with MG132 (Figure 3E). Consistent with a role for SCRAPPER in facilitating degradation of RIM1, untreated brains of SCR-KO mice displayed increased levels of RIM1, which increased further following treatment with MG132, although the relative increase was smaller than that observed after MG132 treatment in WT mice (Figures 3E and 3F). In addition, in MG132-treated IPs from WT mice, RIM1 was shifted to a higher molecular weight, whereas this was not detected in similarly treated IPs from SCR-KO mice (see "RIM1 IP" in Figure 3E). These results indicate that SCRAPPER is the main E3 ligase for RIM1 ubiquitination in a short time window in vivo. Consistent with these findings, the half-life of RIM1 was 0.7 ± 0.1 hr in WT neurons and 5.0 ± 0.1 hr in neurons from SCR-KO mice (Figures 3G, 3H, and S5), confirming that SCRAPPER enhances the rate of turnover of RIM1. In contrast, there was no significant difference in the half-life of β-catenin, an additional synaptic protein (5.4 ± 0.3 hr, WT; 5.0 ± 0.1 hr SCR-KO; Figure S5).

SCRAPPER Regulates the Synaptic Level of RIM1 In Vivo

As the steady-state level of RIM1 was increased in SCR-KO mice, we investigated whether a supraphysiological level of SCRAPPER was sufficient to mediate a decrease in levels of RIM1 in vivo. To do so we performed western analyses of brain lysates from each SCR-TG mouse line (TG-22, TG-26, and TG-31), SCR-KO, and WT mice. Indeed, an increased steady-state level of SCRAPPER produced a reduction in the level of RIM1 as well as several presynaptic proteins, including synaptophysin and synapsin IIa in vivo (Figure 4A). The level of mRNA for presynaptic proteins such as RIM1, synaptotagmin, and SNAP-25 were unchanged in SCR-TG, SCR-KO, and WT mice (Figure S6). In conventional two-dimensional polyacrylamide gel electrophoresis (2D) analyses, almost all brain proteins in SCR-KO and in SCR-TG (data not shown) were unchanged compared with those of WT animals. Thus, the changes of RIM1 protein level in the SCR-KO brain were specific.

Immunofluorescence analyses of SCR-KO hippocampi revealed that the increased level of RIM1 occurred in the synaptic region, not in the cell body (Figures 4B, 4C, and S7). Conversely, the intensity of RIM-specific fluorescence in the synaptic region was reduced in SCR-TG hippocampi relative to that of WT (Figures 4B, 4C, and S7). In parallel, we assessed the distribution and number of synapses of the SCR-KO mice. No significant difference was observed in the number of synapses per neurite length (Figure 4G) between WT and SCR-KO neurons.

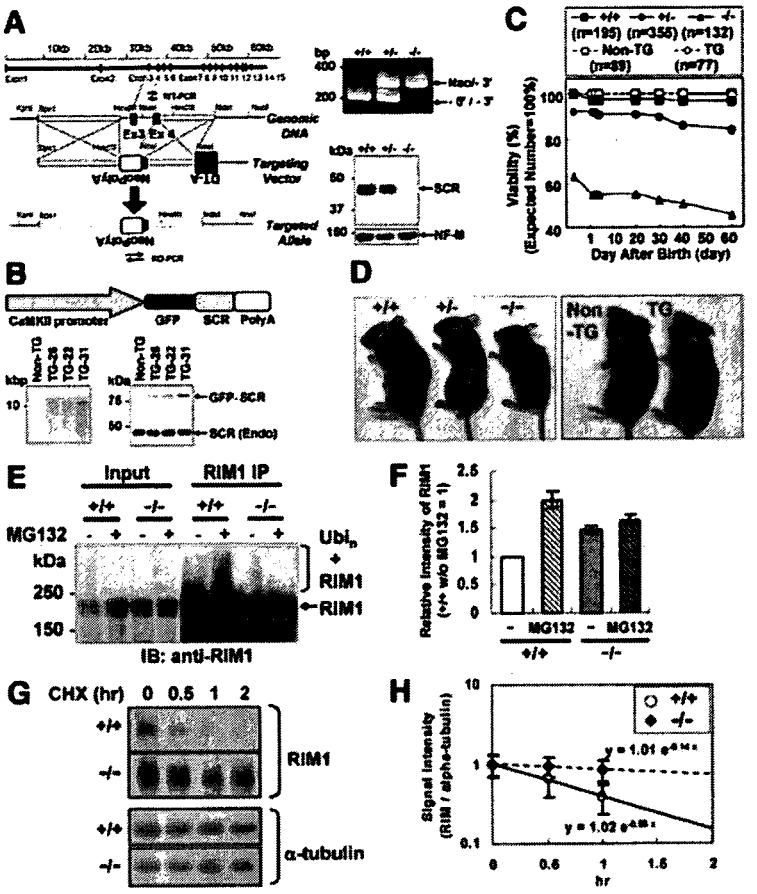

Figure 3. SCRAPPER-Dependent UPS Ubiquitinates RIM1 In Vivo

(A) Targeted disruption of the *Scrapper* gene. Right panels show PCR genotyping and western analysis using anti-SCRAPPER antibody. Neurofilament-M (NF-M) is a loading control.

(B) Upper, cartoon of the transgene; lower panels, Southern blot analysis of genomic DNA from hemizygous mice of indicated TG lines and detection of transgene products using anti-SCRAPPER antibody.

(C) Longevity of SCR-KO mice. Expected ratio of genotypes was based on simple Mendelian rules of inheritance.

(D) Appearance of SCR-KO (left panel) and SCR-TG-31 (right panel) mice.

(E) Ubiquitinated RIM1 was detected in anti-RIM1 immunoprecipitates prepares from acute slices of the WT mice brain treated ±MG132 (50 μM, 1 hr) but not in samples from SCR-KO. Input, original extract; RIM1 IP, immunoprecipitates generated with anti-RIM1 antibody.

(F) Quantification of the relative intensity of RIM1 signal in panel (E), input. Values are means ± SEM (standard error of the mean), n = 3.

(G and H) Increased half-life of RIM1 in SCR-KO neurons. Cultured neurons of cerebral cortex at 7 days in vitro were treated with 20 μg/ml cycloheximide (CHX, a translational inhibitor) for the indicated time period. Values are average signal intensity (means ± SEM, n = 4) of RIM1 compared to signal intensity of α-tubulin and normalized to 1 at time "0." +/+, WT; +/−, heterozygote; −/−, homozygote SCR mutant mice.

Analysis of the hippocampal CA1 region by transmission electron microscopy (TEM) revealed an increased local density and fewer docked synaptic vesicles in SCR-KO neurons (Figures 4D–4F), although the total number of synaptic vesicles was unchanged (Figure 4F). The number of synapses and the sizes of the active zones were also similar in WT and SCR-KO mice (Figure 4F).

SCRAPPER Is a Regulator of Presynaptic Vesicle Release

As RIM1 is known to regulate synaptic transmission (Wang et al., 1997), we investigated whether altered levels of RIM1 and morphological changes of synaptic vesicles in SCR-KO mice was associated with altered neural transmission. We analyzed AMPA-receptor-mediated miniature excitatory postsynaptic currents (mEPSC) from SCR-KO hippocampal primary culture (Inoue et al., 2006). The mEPSC frequency was increased in neurons from SCR-KO mice compared to WT littermates, and the increment was corrected by exogenous re-expression of SCRAPPER (WT; 0.91 ± 0.23 Hz, n = 15, SCR-KO; 3.05 ± 1.12 Hz, n = 14, SCR-KO-rescue; 0.98 ± 0.27 Hz, n = 10) (Figures 5A and 5B). Thus, SCRAPPER plays a significant role in regulation of neurotransmitter release.

To further investigate the functions of SCRAPPER in synaptic transmission via RIM1 ubiquitination, we expressed various forms of GFP-SCRAPPER (Figure 1E) or nontagged red fluorescent protein (RFP) in primary hippocampal neurons (Figure 5C). To determine if SCRAPPER was acting at the pre- or postsynaptic site, we cocultured neurons expressing the various GFP-SCR constructs with neurons expressing only nontagged RFP and recorded mEPSCs. Neurons transfected with GFP-SCR exhibited significant decrease in frequency but not amplitude of mEPSC, whereas the expression of either GFP-SCR-C435A (CAAX mutation) or GFP-SCR-CAAX, which lacks the RIM1 binding domain, had no significant effect on the frequency and amplitude of mEPSC (Figures 5D and 5E). In contrast, neurons transfected with GFP-SCR-LRR, in which we expected a dominant-negative effect caused by binding of the LRR to RIM1, exhibited increased mEPSC frequency but not amplitude (Figures 5D and 5E). Recording of mEPSC from RFP (i.e., non-SCR)-transfected cells in the mixed culture showed the same significant change in mEPSC, demonstrating that the SCRAPPER-dependent effect on neurotransmitter release was generated at the presynaptic site.

Because RIM1 is a known component of a Ca^{2+} sensor (Sudhof, 2004), we tested the Ca^{2+} sensitivity of neurons

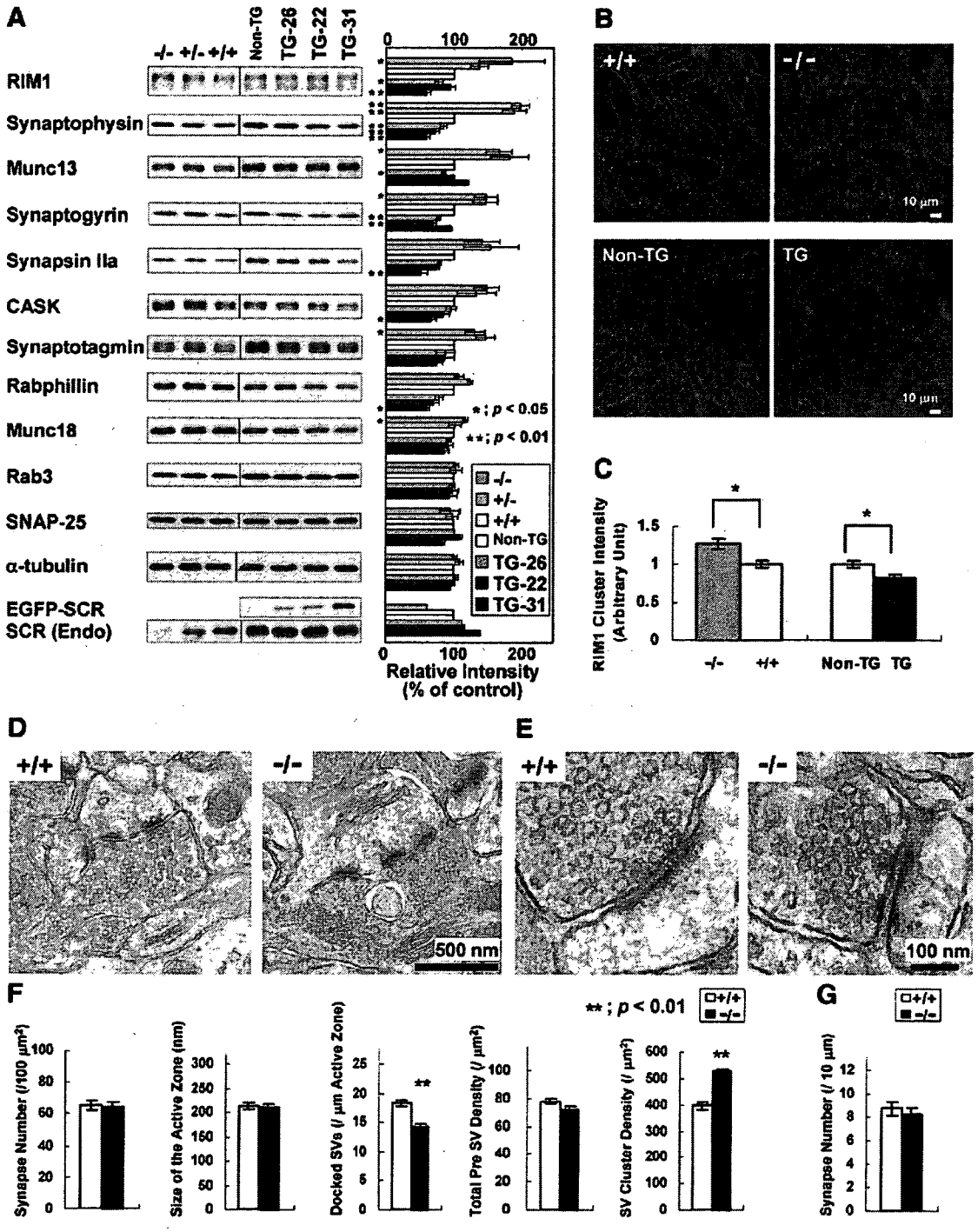

Figure 4. Inverse Relationship between Steady-State Levels of SCRAPPER and a Subset of Presynaptic Proteins In Vivo

(A) Western analysis of SCRAPPER mutant mice. Five μg or 0.5 μg protein of whole brain homogenate was applied to each lane. Values for WT are set at 100%. Three independent animals were analyzed.

(B) Immunofluorescence analyses of hippocampal neurons from WT (+/+), SCR-KO (−/−), non-TG, and SCR-TG-31 (TG) animals labeled with mAb to RIM1 (green) and TOTO-3 (nuclei, blue).

(C) Quantitative analysis of the RIM1 clusters intensity on the panel (B).

(D and E) Representative TEM images of hippocampal CA1 region of WT (+/+) and SCR-KO (−/−) mice.

(F) Quantification of synapses to apical dendrites in the distal stratum radiatum of the hippocampal CA1 region in WT and SCR-KO mice using TEM,

expressing altered forms of SCRAPPER. The effect of expression of SCR forms on modulating mEPSC frequency was observed in the presence of 5 mM but not 10 mM or 20 mM extracellular Ca^{2+} (Figure 5F). Similar results were also observed in the case of evoked-field EPSP (fEPSP) at the hippocampal acute slice preparations (Figures S8A–S8C). We verified that the intracellular Ca^{2+} level of SCR-KO neurons was within the normal range in assays by using Fura2 or a FRET-based Ca^{2+} indicator (Miyawaki et al., 1999) (Figures S8D and S8E). These results indicate that SCRAPPER can regulate the Ca^{2+} sensitivity in presynaptic machinery.

SCRAPPER Regulates Synaptic Vesicle Release via RIM1 and Proteasome Activity

To determine if the altered mEPSC frequency in SCR-KO neurons is mediated specifically via RIM1, we knocked down expression of RIM1 in SCR-KO neurons and analyzed if this was sufficient to rescue the SCR-KO phenotype. Indeed, reduction of RIM1 in SCR-KO neurons was sufficient to rescue the increased frequency of mEPSC (Figures 6A–6C). These results demonstrate that mEPSC frequency can be regulated via SCRAPPER-mediated RIM1 degradation. Overexpression of RIM1 promoted neurotransmitter release (Figures 6D and 6E), which mimicked the SCR-KO phenotype, indicating that the increased RIM1 in SCR-KO mice is sufficient to account for the mEPSC phenotype.

To evaluate the relative contribution of SCRAPPER to UPS-mediated degradation of proteins in neurons, we recorded mEPSC from SCR-KO in the hippocampal CA1 pyramidal neurons in acute slices and analyzed the effect of treatment with MG132 or epoxomicin, another proteasome inhibitor. Significantly, the effect of proteasome inhibitors on mEPSC frequency in acute slices prepared from WT mice was mostly abolished in samples from SCR-KO mice (2.1-fold in WT to 1.2-fold in SCR-KO [MG132 treatment]; 1.9-fold in WT to 1.2-fold in SCR-KO [epoxomicin treatment]; Figure 6H). In contrast, MG132 had no effect on amplitude of mEPSC between SCR-KO and WT mice (Figures 6F–6H).

We investigated the SCRAPPER-proteasome effect on mEPSC not only in acute slices but also in primary cultures of dissociated neurons. When we applied MG132 (50 μM) to primary cultured hippocampal neurons, the frequency and amplitude of mEPSC was increased within 60 min (Figure S9). In contrast, neither amplitude nor frequency of mEPSC was altered following treatment of neurons with the calpain inhibitor ALLM (Figure S9). The mEPSC upregulated by MG132 was completely suppressed under extracellular Ca^{2+}-free conditions and was diminished at higher Ca^{2+} conditions (Figures 6I and 6J). The increase in mEPSC frequency by proteasome inhibitor and the poor response to MG132 in SCR-KO neurons were also demonstrated in the dissociation cultures (7.2-fold in WT to 2.1-fold in SCR-KO, Figure S10).

Altered Short-Term Synaptic Plasticity in SCR-KO Mice

RIM1 mutant mice have increased paired-pulse facilitation (PPF) (Schoch et al., 2002), which is a form of short-term synaptic plasticity (STP) (Katz and Miledi, 1968). Thus, we predicted the PPF in SCR-KO would be affected. We analyzed PPF from the CA3-CA1 synapse of the hippocampal acute slice preparation (Figure 7). The PPF ratio was significantly reduced in SCR-KO mice at every stimulation interval (50, 100, 200, 300, 400, and 500 ms) tested (Figures 7A and 7B). Furthermore, a gradual increase in fEPSP slope and decrease in PPF ratio was observed during treatment of neurons with 50 μM of MG132 for 20 min, and this effect became saturated after 1 hr in both WT and SCR-KO mice (Figures 7C–7E). The effect of exposure to MG132 on fEPSP slope was significantly smaller in SCR-KO mice than in WT mice (normalized fEPSP slope after 1 hr MG132 treatment; 1.31 ± 0.05 in WT, n = 7, versus 1.14 ± 0.04 in KO, n = 7). As with alteration of the mEPSC frequency by MG132 in SCR-KO neurons, the effect of MG132 on the PPF ratio was significantly smaller in SCR-KO mice (i.e., a change from 1.61 ± 0.06 at −10 to 0 min before the application of MG132 to 1.36 ± 0.08 after 1 hr of MG132 treatment, n = 7) compared to WT mice (1.94 ± 0.05 at −10 to 0 min before the application of MG132 to 1.41 ± 0.10 after 1 hr of MG132 treatment, n = 7) (Figures 7D and 7E). These results demonstrate that SCRAPPER can regulate presynaptic STP.

DISCUSSION

SCRAPPER Is an E3 Ligase on Synaptic Membranes

We used bioinformatics to identify SCRAPPER, a neuronal and membranous ubiquitin ligase. SCRAPPER was the only protein identified by our strategy to screen for F box containing proteins that could be membrane localized and whose expression is predicted in neurons. Among the 68 F box protein-coding genes in the human genome (Jin et al., 2004; Winston et al., 1999), *SCRAPPER* is one of six independent genes that have orthologs in *C. elegans*, *D. melanogaster*, and mammals (data not shown), which suggests that it might function as an important membrane-localized E3 ligase in various species. SCRAPPER is broadly expressed within the mouse CNS and is abundant at the presynaptic membrane. Many E3s have been identified whose activities are localized to specific

determined from a total of 230 asymmetrical synapses containing small spherical vesicles and with dense postsynaptic zone from three animals of each genotype.

(G) Quantification of the synapse number per 10 μm neurites of hippocampal neurons. SV, synaptic vesicle. In (A)–(G), data are expressed as means ± SEM. TG, transgenic; +/+, wild-type; −/−, homozygote. *$p < 0.05$; **$p < 0.01$ (t test).

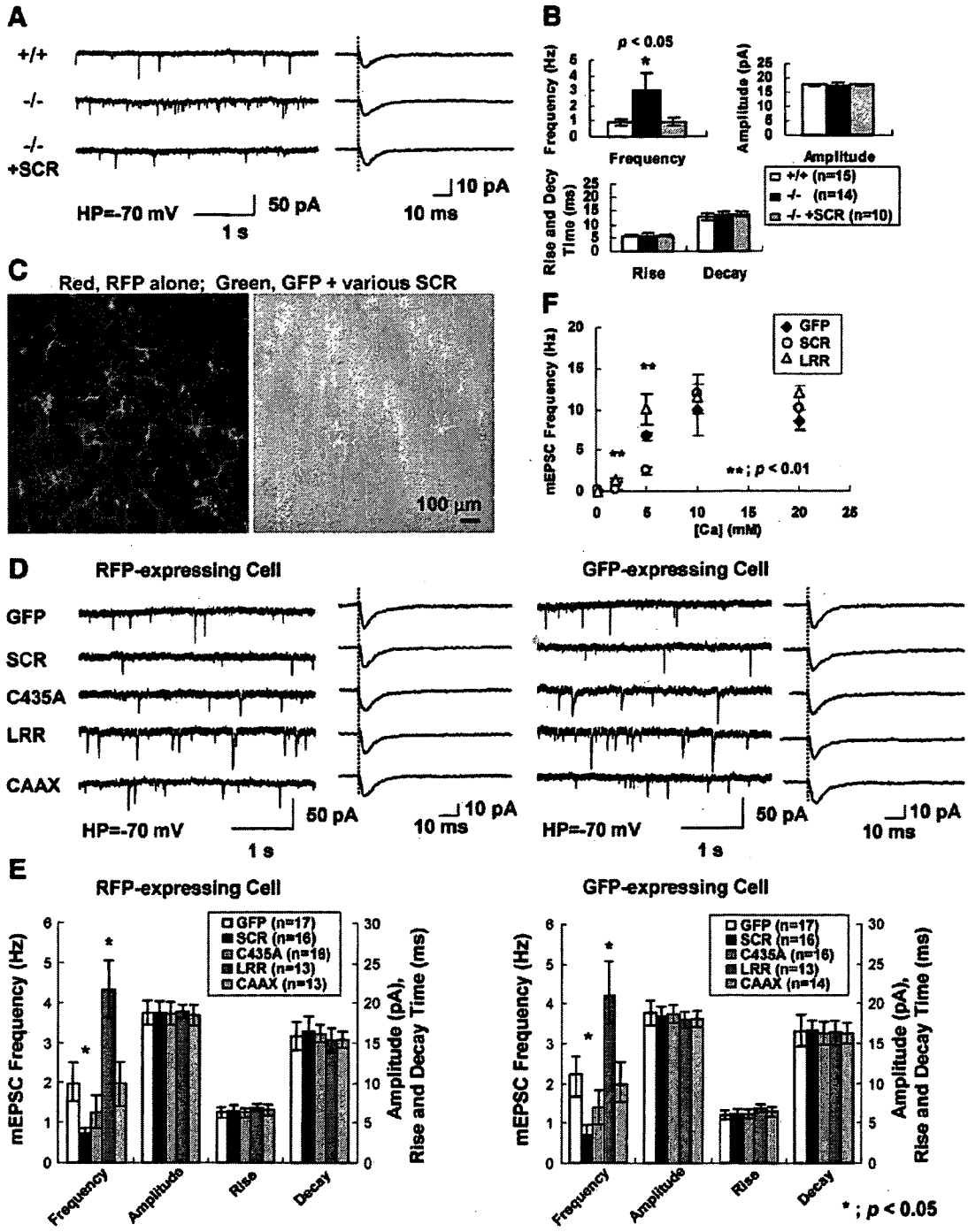

Figure 5. SCRAPPER-Mediated UPS Functions in Presynaptic Transmission

(A) Analysis of mEPSC from hippocampal cultures of SCR-KO (−/−) mice. Representative mEPSC traces for 4 s are in the left column and averaged mEPSC traces are in the right column.

(B) The frequency of mEPSC was significantly increased in the SCR-KO neuron, and the effect was suppressed by re-expression of SCRAPPER.

(C) Representative picture of mixed culture. Rat hippocampal neurons expressing GFP-SCR shown in Figure 1E were cocultured with (control) neurons expressing only nontagged RFP. Right panel is the merge of FL and DIC.

(D) mEPSC was recorded from the nontagged RFP- or GFP-expressing neurons in each group of cocultured neurons. Representative mEPSC trace is in the left column and averaged mEPSC trace is in the right column.

subcellular compartments such as nuclei or cytoplasm, for the regulation of transcription or cell cycles (Coux et al., 1996; Hershko and Ciechanover, 1998).

RIM1 Is a Target of SCRAPPER

Experimentally, SCRAPPER behaves as an F box type E3 ligase and RIM1 is a target of SCRAPPER in the mouse brain. Under normal circumstances, UPS-targeted multiubiquitinated RIM1 are rarely detected due to their rapid turnover. This may account for the relatively weak signal observed of colPed RIM1. Consistent with this prediction, the RIM1-specific signal was shifted upward after in vitro ubiquitination. At present, we cannot exclude the existence of additional SCRAPPER targets in the synapses. Indeed, many E3 enzymes recognize several substrates as a target (Hatanaka et al., 2006b; Ingham et al., 2004).

RIM1 plays an important role in the vesicle priming step in the active zone of the presynapse (Betz et al., 2001; Kaeser and Sudhof, 2005). Recently, we reported that SAD kinase, which can phosphorylate RIM1, is expressed at presynapses and can regulate synaptic transmission (Inoue et al., 2006). Among the F box protein family, the binding of some LRR-type F box proteins to substrates can be influenced by phosphorylation (Hsiung et al., 2001). Because SCRAPPER may recognize the phosphorylation of the substrate as predicted from the leucine-rich sequence, it is possible that SCRAPPER and SAD cooperatively regulate synaptic transmission and plasticity via modulation of RIM1.

Reduction of RIM1 Ubiquitination and Increased Levels of RIM1 in Presynapses in SCR-KO Mice

Analysis of SCR-KO mice revealed that SCRAPPER regulates steady-state level of RIM1. RIM1 degradation can also be controlled via SCRAPPER-independent mechanisms as treatment with MG132, a proteasome inhibitor, produced a further increase in levels of RIM1 in SCR-KO mice. However, the majority of RIM1 degradation appears to be SCRAPPER dependent. This conclusion is supported by the fact that the lifetime of RIM1 was seven times greater in neurons from SCR-KO compared to WT mice. Interestingly, the levels of several presynaptic-localized proteins such as synaptotagmin were also inversely proportional to steady-state level of SCRAPPER in vivo, although the mRNA levels of these presynaptic proteins were unchanged. A 2D analysis indicated that relatively few proteins were affected by the absence of SCRAPPER. This suggests that stabilization of RIM complex proteins in SCR-KO mice impacts relatively few proteins.

Although the sizes of the active zones were unchanged in SCR-KO mice, we found several presynaptic morphological phenotypes such as an increased density of synaptic vesicles and reduced number of docked vesicles. How increased RIM1 generates these morphological phenotypes is not immediately apparent as the synaptic morphology in RIM1-mutant mice does not involve alteration in localization or density of synaptic vesicles (Schoch et al., 2002). The multidomain structure of RIM1 complicates reconciliation of phenotypes in gain- and loss-of-function mice. It is possible that altered expression of presynaptic proteins other than RIM1 contribute to the altered synaptic morphology in SCR KO.

We found no difference in the number and basic structure of synapses in either cultured neurons or hippocampal CA1 region in SCR-KO and WT mice, suggesting that SCRAPPER had no overt effect on synapse development. In contrast, other neural E3 ligase such as *Drosophila* Highwire, the *C. elegans* homolog RPM-1, and the mammalian proteins Phr1 and Pam, constitute a conserved family of proteins, all of which influence synapse development (DiAntonio et al., 2001; McCabe et al., 2004). Additional, as yet unknown E3 ligases may exist that can regulate synaptic development in mammals.

SCRAPPER Is an Important Regulator of Synaptic Transmission

Electrophysiological analyses verified that SCRAPPER can regulate synaptic transmission, especially neurotransmitter release. Recording of mEPSC frequency in mixtures of neurons expressing either nontagged RFP or GFP displayed no significant difference between cells. In contrast, changes observed when recording from nontagged RFP-positive cells in the presence of GFP-positive neurons transfected with different GFP-SCR constructs were interpreted as an effect generated in the presynaptic (green) cell. Use of this strategy (suggested by a reviewer) enabled us to clarify the importance of SCRAPPER function at the presynaptic site. The synapses of neurons expressing elevated levels of SCRAPPER displayed a lower mEPSC frequency via lower Ca^{2+} sensitivity. In contrast, neurons expressing SCR-LRR (RIM1-binding domain) showed a higher Ca^{2+} sensitivity, most likely as a consequence of the dominant-negative effect of this protein. This indicates that SCRAPPER can regulate neurotransmitter release in a LRR domain-dependent manner. This effect was not significantly observed in cells overexpressing SCR-CAAX. Cells expressing SCR-C435A, where the cysteine in the canonical CAAX prenylation motif is replaced by alanine, displayed an intermediate reduction in the frequency of mEPSC, though this was a trend and not statistically significant. One possible explanation why mutation of the cysteine residue diminished SCR activity only moderately is this sequence was able to target SCR to membranes with reduced efficiency.

(E) The frequency of mEPSC recorded from either the nontagged RFP- or GFP-expressing neurons both significantly decreased in GFP-SCR group and increased in GFP-LRR group.

(F) Dependence of extracellular Ca^{2+} concentration on the frequency of the mEPSC. In (B), (E), and (F), data are expressed as means ± SEM. $^{*}p < 0.05$; $^{**}p < 0.01$ (t test).

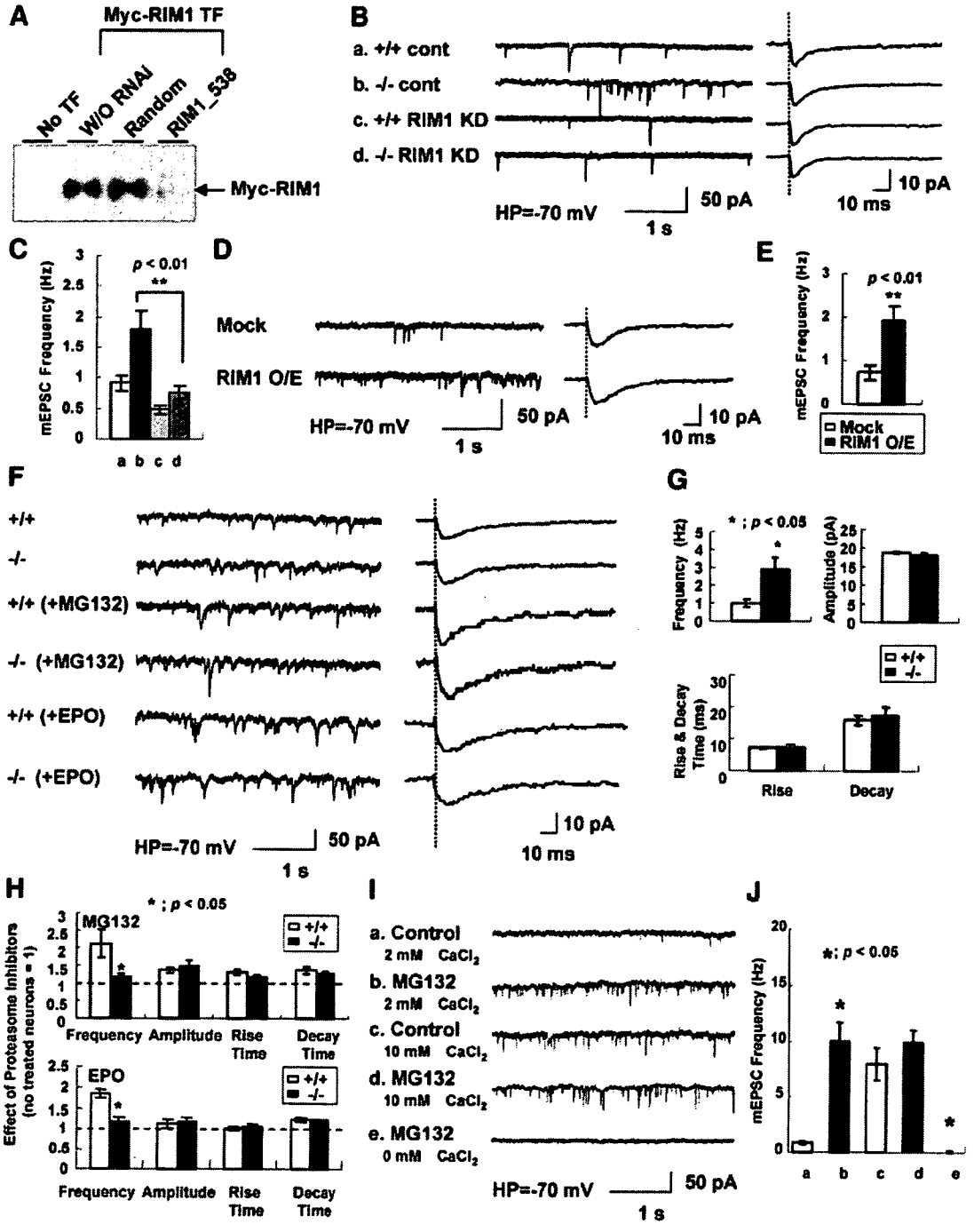

Figure 6. SCRAPPER Tunes Synaptic Transmission via Regulation of RIM1

(A) Western blot analysis of the high efficiency of the knockdown of RIM1with 293T cells ± a vector expressing RNAi against RIM1 (RIM1_538). TF; transfected.

(B) Representative traces of mEPSC from SCR-KO cultured neurons treated ± RIM1-RNAi.

(C) Quantification of mEPSC frequency in (B). Horizontal axis labels correspond to notations in (B).

(D) Representative traces of mEPSC from rat hippocampal cultured neurons transfected with RIM1. O/E, overexpressed.

(E) Comparison of mEPSC frequency in (D).

(F) mEPSC was recorded from CA1 hippocampal neurons of SCR-KO slices (±MG132 [50 μM, 1 hr] or Epoxomicin [10 μM, 1 hr] treatment) under voltage clamp conditions. Representative mEPSC trace (left column); averaged mEPSC trace (right column).

(G) The frequency of mEPSC was significantly increased in the SCR-KO slices compared to the WT.

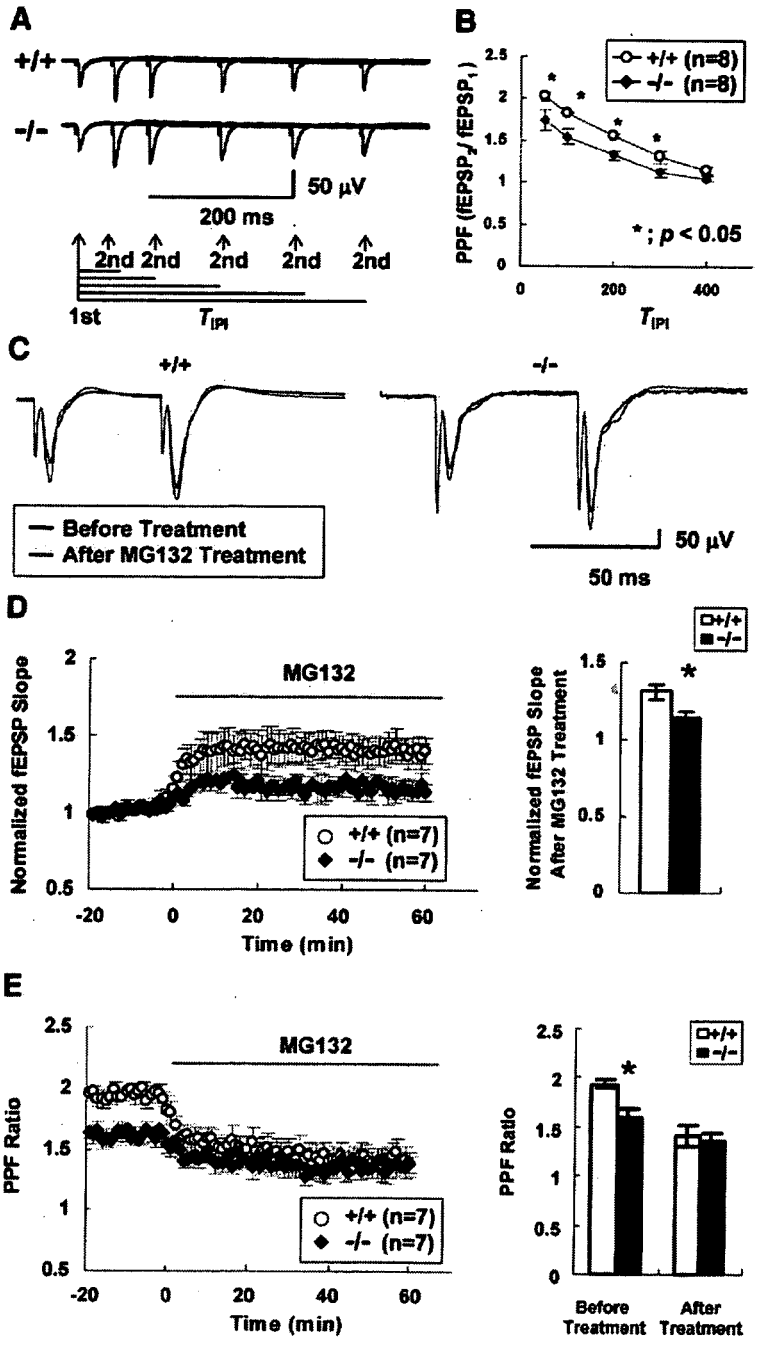

Figure 7. SCRAPPER Functions in Short-Term Synaptic Plasticity

(A and B) PPF ratios of the subsequent and initial fEPSP slopes (interpulse interval: 50, 100, 200, 300, and 400 ms). Data are expressed as means ± SEM.

(C)–(E) Alternation of PPF ratios of the subsequent and initial fEPSP slopes (interpulse interval: 50 ms) recorded from hippocampal slices of WT or SCR-KO mice after treatment with MG132. In (D) and (E), data recorded at 1 min stimulation intervals are expressed as mean ± SEM. *p < 0.05 (t test).

Further experiments are required to discriminate between this and other possibilities. It is possible that the increased mEPSC frequency reduced the number of docked vesicles observed by electron microscopy, and the rate of supply of newly synthesized synaptic vesicles to active zones is unable to support the consumption of synaptic vesicles at the increased mEPSC frequency, although other explanations are possible.

(H) Effect of MG132 (50 μM, 1 hr) or Epoxomicin (10 μM, 1 hr) on mEPSC parameters from the hippocampal slices of WT or SCR-KO mice (n = 3). (I and J) Representative traces of mEPSC from cultured neurons ± MG132 treatment (50 μM, 1 hr) at 0, 2, or 10 mM Ca^{2+} concentration (I) and comparison of mEPSC frequency (J). Horizontal axis labels in panel (I) correspond to the notations in panel (J). Data are expressed as means ± SEM in (C), (E), (G), (H), and (J). *p < 0.05; **p < 0.01 (t test).

The Ca^{2+} sensitivity curve suggests that the targets of the SCRAPPER-proteasome axis should include molecules that regulate Ca^{2+}-dependent neurotransmitter release at the presynapse and that these targets are not molecules such as Ca^{2+} channels, which directly regulate the Ca^{2+} influx, but are likely due to the modulation of the Ca^{2+} sensitivity of presynaptic machinery.

SCRAPPER Regulates Synaptic Transmission via RIM1

Are the effects of loss or gain of function of SCRAPPER on synaptic function mediated specifically through RIM1? RNAi-mediated knockdown of RIM1 in neurons from SCR-KO mice was able to reverse the change in mEPSC, which supports that SCRAPPER does indeed function via RIM1. Moreover, overexpression of RIM1 in WT neurons was sufficient to phenocopy the increased mEPSC frequency in SCR-KO mice. Thus, alteration in steady-state level of RIM1 is sufficient to modulate mEPSC and upstream signaling pathways that function through SCRAPPER can in turn regulate this process. At present we cannot exclude the possibility that monoubiquitination of RIM1 by SCRAPPER may also regulate RIM1 before RIM1 is polyubiquitinated and degraded by the proteasome. Mutation of SCRAPPER abolished the increase in mEPSC observed following treatment of WT neurons with proteasome inhibitors, indicating that SCRAPPER is the major mediator of ongoing proteasomal regulation of mEPSC frequency. The rapidity of MG132 action suggests that the effects are independent of transcriptional regulation. These results also indicate that there is robust proteasome activity for the regulation of Ca^{2+}-dependent synaptic vesicle release.

SCRAPPER Contributes to Regulation of Synaptic Plasticity

Synaptic plasticity is thought to be an important basis for learning and memory (Brown et al., 1990). PPF is one form of STP, the fundamental basis of synaptic plasticity. Ataxin-1 knockout mice show learning deficits and decreased hippocampal PPF, despite having normal LTP induction (Matilla et al., 1998). This indicates that PPF is related to learning. We showed that SCRAPPER functions as a regulator of PPF (i.e., synaptic plasticity), at presynapses.

SCR-KO mice displayed decreased PPF ratio. In addition, MG132-dependent upregulation of fEPSP was suppressed in SCR-KO animals. Our findings demonstrate that UPS-dependent regulation of PPF and mEPSC is mainly controlled by SCRAPPER. Based on analysis of RIM1 knockout mice in which the PPF value was increased at the hippocampal CA1 synapse (Schoch et al., 2002), together with the increased steady-state level of RIM1 in SCR-KO mice, we propose that increased RIM1 is a major contributor to the decreased PPF observed in SCR-KO mice. Thus, SCRAPPER appears to induce degradation of RIM1 complex via the proteasome, which regulates the PPF ratio. We note that overexpression of Munc13 also increases mEPSC (Betz et al., 1998) and that synaptotagmin I increased the probability of vesicle fusion (Kreft et al., 2003). Hence, it is formally possible that upregulation of Munc13 and synaptotagmin could also contribute to the changes of PPF and mEPSC in SCR-KO mice.

Neural activity-dependent alteration of *Scrapper* expression directly implicates SCRAPPER as being involved in neural activity-dependent protein degradation, which in turn alters synaptic transmission efficiency. Regulation of RIM1 protein complex level is likely to cause both short- and long-term changes in the PPF ratio. That SCRAPPER can facilitate a long-term change in synaptic efficacy suggests that SCRAPPER could influence regulation of "the plasticity of plasticity" at the presynapse—i.e., the metaplasticity (Abraham and Tate, 1997). We have focused our investigation on presynaptic functions. However, as SCRAPPER is also localized to dendrites, there may be additional effects of SCRAPPER disruption on neuronal function and postsynaptic function. Finally, we speculate that the activation of certain neural networks does not occur in SCR-KO, because SCRAPPER may also serve as E3 for an unknown substrate in inhibitory neurons, which in turn may give rise to the inactivation of a certain population of excitatory neurons. In summary, we have identified a physiological role of SCRAPPER-dependent RIM1 ubiquitination for proteasomal degradation in presynaptic function. Many kinds of neuronal disorder/disease are caused by excessive neurotransmitter release. An attractive possibility is that SCRAPPER can be a potential target of new drug designs for the treatment of neuronal diseases.

EXPERIMENTAL PROCEDURES

Identification of SCRAPPER and Cloning of *Scrapper* Gene

Eleven hundred thirty genes with both neuron-restrictive silencing element and cAMP-response element were found using the Celera Discovery System (a search program that is no longer available). The F box domain was identified by the Pfam program. Cloning of the *Scrapper* gene was performed by RT-PCR, using cDNA from newborn mouse brain and *Scrapper*-specific primers. The NCBI accession number of *Scrapper* is EF649694.

Animals

Care and experiments with animals were in accordance with institutional guidelines and those of the National Institute of Health and the Animal Care and Use Committee (Mitsubishi Kagaku Institute of Life Science). C57BL/6 mice and Wistar SD rats were used.

Antibodies

Rabbit anti-SCRAPPER antibody was raised against amino residues 321–380 of mouse SCRAPPER expressed in bacteria. Other antibodies used are described in the Supplemental Data.

Miscellaneous Procedures

In situ hybridization for *Scrapper* mRNA was performed as described (Ikegami et al., 2006). Details are described in the Supplemental Data. Plasmid construction, cell culture, and Southern and western blotting were performed by conventional methods (Hatanaka et al., 2006c). Subcellular fractionation of mouse brain was performed as

described (Yao et al., 1999). Fractions were analyzed by western blotting. Stability of RIM1 was measured by the treatment of 20 μg/ml cycloheximide (Hatanaka et al., 2006a) to cerebral cortical primary culture from WT or SCR-KO mice. RIM1 was knockdowned by the miR-RNAi system (Invitrogen).

Neuron Culture and Immunostaining

Hippocampal neurons were prepared (Kato et al., 2001) with minor modifications described in the Supplemental Data. Cultured cells were transfected with 1 μg DNA with Lipoofectamine2000 (Invitrogen). Primary cultured neurons from SCR-KO mice were prepared with P1–P3 mice. Immunofluorescence and immunohistochemical studies were performed as described (Yao et al., 2002) and imaged and quantified using confocal microscopy operated under manual control (Zeiss LSM5 PASCAL, Olympus FV-1000). For mixed culture, neurons were incubated separately with each DNA mixture, subsequently washed to remove any adherent DNA before plating then cocultured. The cells transfected independently with a vector expressing either nontagged RFP (DsRed2, Clontech), or different GFP-SCR constructs were plated together with other group neurons and used at 12–15 days in vitro for electrophysiological recordings. The mEPSC frequency recorded form neurons expressing either nontagged RFP or nontagged GFP displayed no significant difference between cells. The changes observed when recording from Red cells in the presence of green neurons transfected with different GFP-SCR constructs were interpreted as an effect generated in the presynaptic (green) cell.

Immunoprecipitation and In Vitro Pull-Down Assay

Immunoprecipitation of the mouse brain was performed as described (Yao et al., 1999). HEK293T cells were lysed 48 hr after transfection with a solution containing 50 mM Tris-Cl (pH 7.4), 100 mM NaCl, 1% (v/v) Triton X-100, and a cocktail of protease inhibitors (Complete EDTA-free, Roche). Cell lysates were incubated with 5 μg of antibody in 10 μl of protein G-sepharose beads (Amersham) for 4 hr at 4°C. Immunoprecipitates were washed four times with ice-cold lysis buffer and were blotted with appropriate antibodies. In vitro binding using GST fusion proteins and cell extract was performed as described (Yao et al., 1999).

In Vitro Immunoprecipitation and Ubiquitination Assays

Recombinant Uba1 (E1), GST-UbcH5 (E2), Hisx6-ubiquitin, APP-BP1/Uba3, GST-UbcH12, and NEDD8 were purchased from Medical and Biological laboratories Company, Limited. The NEDD8 system containing APPBP1/Uba3, UbcH12, and NEDD8 was added simultaneously to the mixture. SCRAPPER was immunoprecipitated with anti-SCRAPPER conjugated to Protein G sepharose, and denatured after being washed three times. The ubiquitination assay was carried out as described (Kawakami et al., 2001).

***SCRAPPER* Knockout and Transgenic Mice**

We used homologous recombination in ES cells to mutate *Scrapper*. Exon 3 (which encodes the region including the F box domain) and a part of exon 4 (a recombination that generates a frameshift) were replaced by a Neo selection cassette. Analysis of SCR-KO mice was performed on littermates derived from mating heterozygous mutant mice on a hybrid 129Sv/C57BL6 background and was confirmed with several independent litters derived from independent generations of heterozygous breeding. We established three independent mouse lines overexpressing GFP-fused SCRAPPER (TG-22, TG-26, and TG-31). The GFP-SCRAPPER transgene contains a CaMKII promoter, an EGFP tag, a *Scrapper*-coding region, and a polyadenylation signal. Details are described in the Supplemental Data. Two-dimensional analyses of the brain homogenate of *Scrapper* knockout mice were performed as described (Omori et al., 2002).

Transmission Electron Microscopy

Transmission electron microscopy (TEM) was performed as described (Ikegami et al., 2006) and in the Supplemental Data. Quantitative analysis of TEM micrographs was performed as described (Altrock et al., 2003; Schoch et al., 2002).

Recording of mEPSC

mEPSC was recorded as described (Inoue et al., 2006), see the Supplemental Data. Cells for whole-cell recording configuration were selected on the status of RFP or GFP expression. The average frequency (Hz), amplitude (pA), rise time (ms), and decay time (ms) from each neuron were then averaged to give a value for the entire population. Statistical significance was determined using the two-tailed, paired Student's t test. $^*p < 0.05$ was considered to be statistically significant.

Electrophysiology of Hippocampal Slices

Hippocampal 300-μm-thickness slices were prepared from ether-anesthetized 3- to 4-week-old SCR-KO mice as described in the Supplemental Data. PPF was measured by using two-paired 50, 100, 200, 300, and 400-ms interpulse interval stimuli. The PPF ratio ($2^{nd}/1^{st}$ fEPSP slope) was evaluated in each interpulse interval (IPI).

Supplemental Data

Supplemental Data include Supplemental Experimental Procedures, Supplemental References, and ten figures and can be found with this article online at http://www.cell.com/cgi/content/full/130/5/943/DC1/.

ACKNOWLEDGMENTS

We are grateful to K. Nakamura, R. Migishima, and T. Hino, Mouse Genome Technology Center at MITILS, for generating SCR-KO and SCR-TG mice. We also wish to thank T. Sekiya, S. Song, A. Omori, S. Kamiyo, and K. Nagayama and M. Arai, Y. F.-Tsukamoto, Y. Hinohara, and other members of the Setou group and MITILS. We thank Profs. Mayford and Kida for the CaMKII promoter vector, Dr. Seino for the RIM1 constructs, and Ms. Takamura for critical reading of this manuscript. We thank three anonymous reviewers for constructive criticism and superb suggestions for experiments to strengthen the study. This work was supported by Research Grants for PRESTO and SENTAN, from JST and a Grant-in-Aid for Young Scientists A to M.S., by a Grant-in-Aid for Young Scientists B to I.Y., by NANO-001 (N.M.), NIBIO 05-32 (S.Y.) to N.M., and in part by a grant from company, MITILS. A portion of this study was presented at 46th Annual Meeting of the ASCB.

Received: January 25, 2007
Revised: May 1, 2007
Accepted: June 18, 2007
Published: September 6, 2007

REFERENCES

Abraham, W.C., and Tate, W.P. (1997). Metaplasticity: a new vista across the field of synaptic plasticity. Prog. Neurobiol. *52*, 303–323.

Ageta, H., Kato, A., Hatakeyama, S., Nakayama, K., Isojima, Y., and Sugiyama, H. (2001). Regulation of the level of Vesl-1S/Homer-1a proteins by ubiquitin-proteasome proteolytic systems. J. Biol. Chem. *276*, 15893–15897.

Altrock, W.D., tom Dieck, S., Sokolov, M., Meyer, A.C., Sigler, A., Brakebusch, C., Fassler, R., Richter, K., Boeckers, T.M., Potschka, H., et al. (2003). Functional inactivation of a fraction of excitatory synapses in mice deficient for the active zone protein bassoon. Neuron *37*, 787–800.